JAERI-M
84-005

X-RAY PHOTOELECTRON AND X-RAY-INDUCED AUGER ELECTRON SPECTROSCOPIC DATA, I

—3d TRANSITION-METALS(Sc, Ti, V, Ni) AND RELATED OXIDES—

February 1984

Yuji BABA and Teikichi A. SASAKI

日本原子力研究所
Japan Atomic Energy Research Institute

JAERI-M レポートは，日本原子力研究所が不定期に公刊している研究報告書です。
入手の問合わせは，日本原子力研究所技術情報部情報資料課（〒319—11 茨城県那珂郡東海村）あて，お申しこしください。なお，このほかに財団法人原子力弘済会資料センター（〒319-11 茨城県那珂郡東海村日本原子力研究所内）で複写による実費頒布をおこなっております。

JAERI-M reports are issued irregularly.
Inquiries about availability of the reports should be addressed to Information Section, Division of Technical Information, Japan Atomic Energy Research Institute, Tokai-mura, Naka-gun, Ibaraki-ken 319-11, Japan.

編集兼発行　日本原子力研究所
印　　刷　山田軽印刷所

JAERI-M 84-005

X-RAY PHOTOELECTRON AND X-RAY-INDUCED AUGER ELECTRON SPECTROSCOPIC DATA, I — 3d TRANSITION-METALS (Sc, Ti, V, Ni) AND RELATED OXIDES —

Yuji BABA and Teikichi A. SASAKI

Department of Chemistry, Tokai Research Establishment, JAERI

(Received January 17, 1984)

The intrinsic data of the X-ray photoelectron spectra (XPS) and X-ray-induced Auger electron spectra (XAES) for 3d transition-metals and related oxides were presented. The clean surfaces of the metals were obtained by two different methods ; mechanical filings and Ar^+ ion etchings. The oxides examined are typical compounds such as Sc_2O_3, TiO_2, V_2O_5 and NiO. The report consists of 4 wide scans, 26 core-line spectra, 10 valence-band spectra and 20 XAES spectra. The peak positions of the core-lines and the Auger lines were summarized in 8 tables together with their chemical shifts.

KEYWORDS :

X-ray Photoelectron Spectroscopy, X-ray-induced Auger Electron Spectroscopy, Scandium, Titanium, Vanadium, Nickel, Oxides, Sputtering

---

This work was done by the use of an ESCA spectrometer connected with the JAERI Tandem Accelerator.

JAERI-M 84-005

X線光電子分光及びX線励起オージェ電子スペクトル，データ集I
－3d遷移金属（Sc，Ti，V，Ni）及びその酸化物－

日本原子力研究所東海研究所原子炉化学部
馬場　祐治・佐々木　貞吉

（1984年1月17日受理）

3d遷移金属とその酸化物固有のX線光電子分光スペクトル（XPS）及びX線励起オージェ電子スペクトル（XAES）を測定した。金属の真正表面は2通りの異なる方法，すなわち超高真空中やすり研摩法及びアルゴンイオンエッチング法で得た。測定した金属酸化物はSc_2O_3，TiO_2，V_2O_5，NiOである。本報は4種のワイドスキャン，26種の内殻スペクトル，10種の価電子帯スペクトル及び20種のXAESスペクトルから成る。内殻及びオージェピークの位置については，その化学シフトと共に表にまとめた。

LIST OF TABLES

---

* : Notation *fl* indicates a mechanical filing.

** : Notation *et* indicates an Ar^+ ion etching.

LIST OF FIGURES

Contents

目　　次

1. Introduction

X-ray photoelectron spectroscopy (XPS) is widely used for the chemical state analyses of solid surfaces. The intrinsic data of the XPS spectra which are available for the studies of material science have been compiled for many elements and their typical compounds as a handbook.[1] The chemical shifts of the main core-lines have also been summarized in tables.[1,2]

However, the intrinsic data of the valence-band and the other core-line spectra with relatively weak intensities have not been compiled yet. In addition, the handbooks published are not necessarily comprehensive in their coverages. One of the objects in this series of the reports is to present the intrinsic features of the XPS spectra newly obtained both for valence-band regions and for various core-lines.

Another aim of the reports is to display the data of the X-ray-induced Auger electron spectroscopy (XAES). This method has been revealed to be often more effective in analyzing the surface chemical states than the XPS, since there exist many examples that the chemical shifts of the Auger lines are larger than those of the corresponding core-line photopeaks. The XAES chemical shifts so far obtained have been summarized in terms of the Auger parameter.[1,3,4] However, the available data of the chemical shifts are rather scarce, compared with those of the XPS.

In this report, the XPS and XAES spectra for some 3d transition-metals (Sc, Ti, V, Ni) and their typical oxides are presented. Although many XPS spectra for these metals have been published, clean surface of the metals has been obtained mostly by Ar^+ ion etching. However, it must be emphasized that the bombardment of the heavy ions may cause the lattice distortion of the metal surface, resulting in the spectral changes of the XPS or XAES. In the present study, therefore, the clean surfaces of the metals were obtained mainly by mechanical filings under the ultra-high vacuum conditions. For comparison, the spectra for the metal surfaces etched with the Ar^+ ions were also given.

2. Preparation of samples

Starting materials used were 99.9 % metallic foils. The clean surfaces of the metals were obtained by two different methods. One is a mechanical filing in a preparation chamber under the pressure of 1.3×10^{-8} Pa, and another is an Ar^+ ion etching. The latter method was done by bombarding the mechanically filed metals with 8 keV Ar^+ ions at a current density of $\sim$20 $\mu A/cm^2$ for 30 min.

The oxides such as Sc_2O_3, TiO_2, V_2O_5 and NiO were prepared by oxidizing the metallic foils at 300-400°C in an oxygen atmosphere. Before the spectral measurements, the oxide samples were heated at 200°C in the spectrometer chamber under the pressure of $\sim1.3\times10^{-7}$ Pa.

3. Spectral measurements

The XPS and XAES measurements were carried out by the use of a V.G. ESCALAB-5 spectrometer, under the pressure of less than 1.3×10^{-8} Pa. A Mg $K\alpha$ X-ray source (1253.6 eV) was operated at 125 W. The spectrometer was calibrated such that the Au $4f_{7/2}$ line appears at E_b=84.0 eV. The FWHM (full-width at half maximum) of the Au $4f_{7/2}$ line was 0.9 eV, and the reproducibility of the spectrometer was within ±0.1 eV. In the case of the insulating oxides, the original spectra shifted to the higher binding-energy side because of charging effect. Therefore the energy scale was aligned to make the peak positions of the Me $2p_{1/2}$ lines for the oxides and for the most oxidized species on the oxygen-adsorbed surfaces coinside.

4. Results

In the tables and figures, the notations *fl* and *et* represent the mechanical filing and the Ar^+ ion etching, respectively. The XPS and XAES spectra for Sc_{fl}, Sc_{et} and Sc_2O_3 are presented in Figs. 1-18, for Ti_{fl}, Ti_{et} and TiO_2 in Figs. 19-32, for V_{fl}, V_{et} and V_2O_5 in Figs. 33-49, and for Ni_{fl}

2. Preparation of samples

Starting materials used were 99.9 % metallic foils. The clean surfaces of the metals were obtained by two different methods. One is a mechanical filing in a preparation chamber under the pressure of 1.3×10^{-8} Pa, and another is an Ar^+ ion etching. The latter method was done by bombarding the mechanically filed metals with 8 keV Ar^+ ions at a current density of $\sim$20 $\mu A/cm^2$ for 30 min.

The oxides such as Sc_2O_3, TiO_2, V_2O_5 and NiO were prepared by oxidizing the metallic foils at 300-400 °C in an oxygen atmosphere. Before the spectral measurements, the oxide samples were heated at 200 °C in the spectrometer chamber under the pressure of $\sim1.3\times10^{-7}$ Pa.

3. Spectral measurements

The XPS and XAES measurements were carried out by the use of a V.G. ESCALAB-5 spectrometer, under the pressure of less than 1.3×10^{-8} Pa. A Mg K_α X-ray source (1253.6 eV) was operated at 125 W. The spectrometer was calibrated such that the Au $4f_{7/2}$ line appears at E_b=84.0 eV. The FWHM (full-width at half maximum) of the Au $4f_{7/2}$ line was 0.9 eV, and the reproducibility of the spectrometer was within ±0.1 eV. In the case of the insulating oxides, the original spectra shifted to the higher binding-energy side because of charging effect. Therefore the energy scale was aligned to make the peak positions of the Me $2p_{1/2}$ lines for the oxides and for the most oxidized species on the oxygen-adsorbed surfaces coinside.

4. Results

In the tables and figures, the notations *fl* and *et* represent the mechanical filing and the Ar^+ ion etching, respectively. The XPS and XAES spectra for Sc_{fl}, Sc_{et} and Sc_2O_3 are presented in Figs. 1-18, for Ti_{fl}, Ti_{et} and TiO_2 in Figs. 19-32, for V_{fl}, V_{et} and V_2O_5 in Figs. 33-49, and for Ni_{fl}

2. Preparation of samples

Starting materials used were 99.9 % metallic foils. The clean surfaces of the metals were obtained by two different methods. One is a mechanical filing in a preparation chamber under the pressure of 1.3×10^{-8} Pa, and another is an Ar^+ ion etching. The latter method was done by bombarding the mechanically filed metals with 8 keV Ar^+ ions at a current density of $\sim$20 $\mu A/cm^2$ for 30 min.

The oxides such as Sc_2O_3, TiO_2, V_2O_5 and NiO were prepared by oxidizing the metallic foils at 300-400 °C in an oxygen atmosphere. Before the spectral measurements, the oxide samples were heated at 200 °C in the spectrometer chamber under the pressure of $\sim1.3\times10^{-7}$ Pa.

3. Spectral measurements

The XPS and XAES measurements were carried out by the use of a V.G. ESCALAB-5 spectrometer, under the pressure of less than 1.3×10^{-8} Pa. A Mg K_α X-ray source (1253.6 eV) was operated at 125 W. The spectrometer was calibrated such that the Au $4f_{7/2}$ line appears at E_b=84.0 eV. The FWHM (full-width at half maximum) of the Au $4f_{7/2}$ line was 0.9 eV, and the reproducibility of the spectrometer was within ±0.1 eV. In the case of the insulating oxides, the original spectra shifted to the higher binding-energy side because of charging effect. Therefore the energy scale was aligned to make the peak positions of the Me $2p_{1/2}$ lines for the oxides and for the most oxidized species on the oxygen-adsorbed surfaces coinside.

4. Results

In the tables and figures, the notations *fl* and *et* represent the mechanical filing and the Ar^+ ion etching, respectively. The XPS and XAES spectra for Sc_{fl}, Sc_{et} and Sc_2O_3 are presented in Figs. 1-18, for Ti_{fl}, Ti_{et} and TiO_2 in Figs. 19-32, for V_{fl}, V_{et} and V_2O_5 in Figs. 33-49, and for Ni_{fl}

, Ni_{et} and NiO in Figs. 50-60, respectively. In these figures, the peak positions are indicated in eV. The binding energies of the core-lines are summarized in Tables 1-4 and the kinetic energies of the Auger lines are listed in Tables 5-8.

REFERENCES

1) Wagner C. D., Riggs W. M., Davis L. E., Moulder J. F. and Mullenberg G. E. : "Handbook of X-ray Photoelectron Spectroscopy", Perkin-Elmer Corporation, Minnesota (1979).
2) Robinson J. W. : "Handbook of Spectroscopy", Chemical Rubber Company, Ohio, Vol. 1, 517 (1974).
3) Wagner C. D. : Faraday Discuss. Chem. Soc., 60, 291 (1975).
4) Wagner C. D., Gale L. H. and Raymond R. H. : Anal. Chem., 51, 466 (1979).

, Ni_{et} and NiO in Figs. 50-60, respectively. In these figures, the peak positions are indicated in eV. The binding energies of the core-lines are summarized in Tables 1-4 and the kinetic energies of the Auger lines are listed in Tables 5-8.

REFERENCES

1) Wagner C. D., Riggs W. M., Davis L. E., Moulder J. F. and Mullenberg G. E. : "Handbook of X-ray Photoelectron Spectroscopy", Perkin-Elmer Corporation, Minnesota (1979).
2) Robinson J. W. : "Handbook of Spectroscopy", Chemical Rubber Company, Ohio, Vol. 1, 517 (1974).
3) Wagner C. D. : Faraday Discuss. Chem. Soc., 60, 291 (1975).
4) Wagner C. D., Gale L. H. and Raymond R. H. : Anal. Chem., 51, 466 (1979).

Table 1 Binding energies and chemical shifts of the core-lines for Sc_{fl}, Sc_{et} and Sc_2O_3.

Sample	Orbital	E_b (eV)	Chemical Shift (eV)	Fig. No.
Sc_{fl}	2s	498.5	-	2
	$2p_{1/2}$	403.6	-	3
	$2p_{3/2}$	398.8	-	3
	3s	51.3	-	4
	3p	28.5	-	5
Sc_{et}	$2p_{1/2}$	398.8	0.0	9
	$2p_{3/2}$	403.7	0.1	9
Sc_2O_3	2s	501.8	3.3	12
	$2p_{1/2}$	407.4	3.8	13
	$2p_{3/2}$	403.0	4.2	13
	3s	54.2	2.9	14
	3p	32.4	3.9	15

Table 2 Binding energies and chemical shifts of the core-lines for Ti_{fl}, Ti_{et} and TiO_2.

Sample	Orbital	E_b (eV)	Chemical Shift (eV)	Fig. No.
Ti_{fl}	$2p_{1/2}$	460.3	-	20
	$2p_{3/2}$	454.2	-	20
	3s	58.9	-	21
	3p	33.0	-	22
Ti_{et}	$2p_{1/2}$	460.6	0.3	25
	$2p_{3/2}$	454.5	0.3	25
TiO_2	$2p_{1/2}$	464.7	4.4	28
	$2p_{3/2}$	459.0	4.8	28
	3s	62.3	3.4	29
	3p	37.4	4.4	30

Table 3 Binding energies and chemical shifts of the core-lines for V_{fl}, V_{et} and V_2O_5.

Sample	Orbital	E_b (eV)	Chemical Shift (eV)	Fig. No.
V_{fl}	$2p_{1/2}$	519.8	-	34
	$2p_{3/2}$	512.1	-	34
	3s	66.1	-	35
	3p	37.0	-	36
V_{et}	$2p_{1/2}$	519.9	0.1	40
	$2p_{3/2}$	512.4	0.3	40
V_2O_5	$2p_{1/2}$	524.5	4.7	44
	$2p_{3/2}$	517.0	4.9	44
	3s	70.1	4.0	45
	3p	42.0	5.0	46

Table 4 Binding energies and chemical shifts of the core-lines for Ni_{fl}, Ni_{et} and NiO.

Sample	Orbital	E_b (eV)	Chemical Shift (eV)	Fig. No.
Ni_{fl}	$2p_{1/2}$	870.2	-	51
	$2p_{3/2}$	853.0	-	51
Ni_{et}	$2p_{1/2}$	870.1	-0.1	56
	$2p_{3/2}$	852.9	-0.1	56
NiO	$2p_{1/2}$	873.3	3.1	58
	$2p_{3/2}$	854.6	1.6	58

Table 5 Kinetic energies and chemical shifts of the Auger lines for Sc_{fl}, Sc_{et} and Sc_2O_3.

Sample	Transition	E_k (eV)	Chemical Shift (eV)	Fig. No.
Sc_{fl}	$L_{2,3}M_{2,3}M_{2,3}$	337.0	-	7
	$L_{2,3}M_{2,3}V$	368.9	-	8
Sc_{et}	$L_{2,3}M_{2,3}M_{2,3}$	337.3	-0.3	10
	$L_{2,3}M_{2,3}V$	368.9	0.0	11
Sc_2O_3	$L_{2,3}M_{2,3}M_{2,3}$	333.0	4.0	17
	$L_{2,3}M_{2,3}V$	361.4	7.5	18

Table 6 Kinetic energies and chemical shifts of the Auger lines for Ti_{fl}, Ti_{et} and TiO_2.

Sample	Transition	E_k (eV)	Chemical Shift (eV)	Fig. No.
Ti_{fl}	$L_3M_{2,3}V$	418.9	-	24
Ti_{et}	$L_3M_{2,3}V$	419.0	-0.1	27
TiO_2	$L_3M_{2,3}V$	419.0	-0.1	32

Table 7 Kinetic energies and chemical shifts of the Auger lines for V_{fl}, V_{et} and V_2O_5.

Sample	Transition	E_k (eV)	Chemical Shift (eV)	Fig. No.
V_{fl}	$L_3M_{2,3}M_{2,3}$	438.2	-	38
	$L_3M_{2,3}V$	472.1	-	39
V_{et}	$L_3M_{2,3}M_{2,3}$	438.0	0.2	42
	$L_3M_{2,3}V$	472.1	0.0	43
V_2O_5	$L_3M_{2,3}M_{2,3}$	432.5	5.7	48
	$L_3M_{2,3}M_{2,3}$	466.9	5.2	49

Table 8 Kinetic energies and chemical shifts of the Auger lines for Ni_{fl}, Ni_{et} and NiO.

Sample	Transition	E_k (eV)	Chemical Shift (eV)	Fig. No.
Ni_{fl}	$L_3M_{2,3}M_{2,3}$	708.2	-	53
	$L_3M_{2,3}V$	774.0	-	54
	L_3VV	845.7	-	55
Ni_{et}	L_3VV	846.0	-0.3	57
NiO	L_3VV	843.1	2.6	60

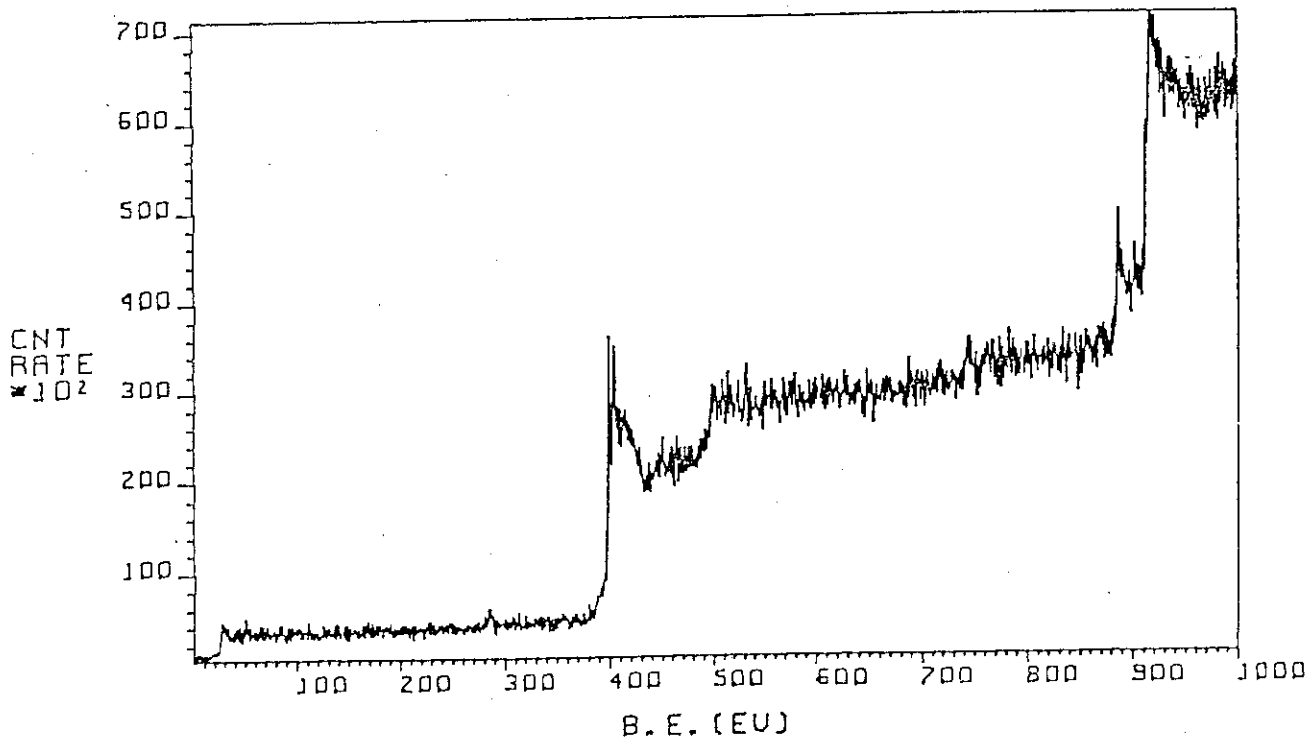

Fig. 1 XPS wide scan of Sc$_{fl}$.

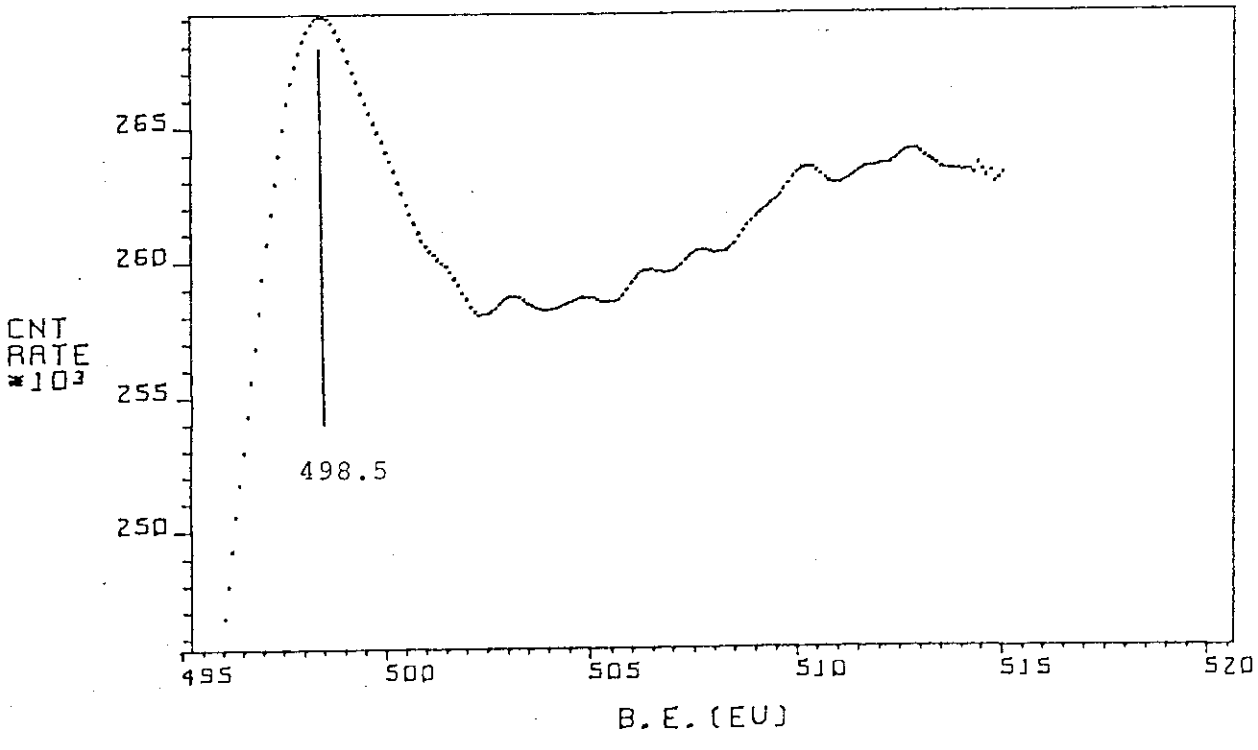

Fig. 2 Sc2s XPS spectrum of Sc$_{fl}$.

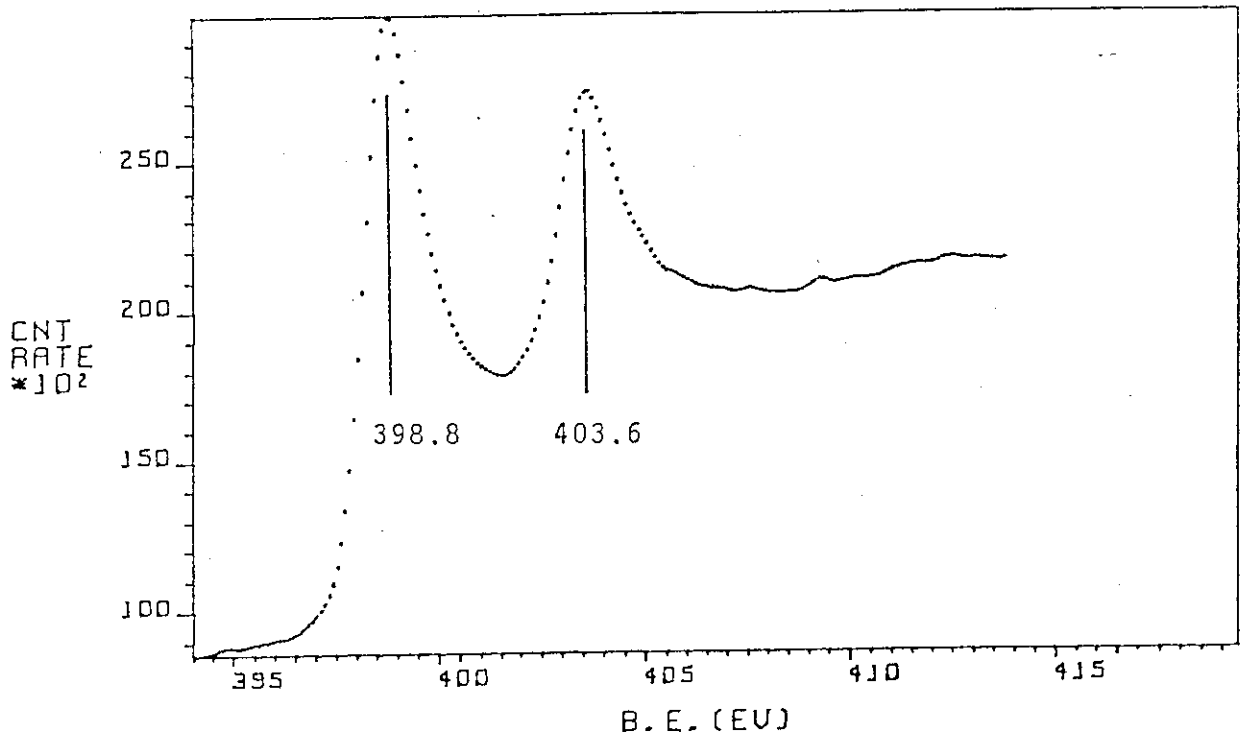

Fig. 3 Sc2p XPS spectrum of Sc_{fl}.

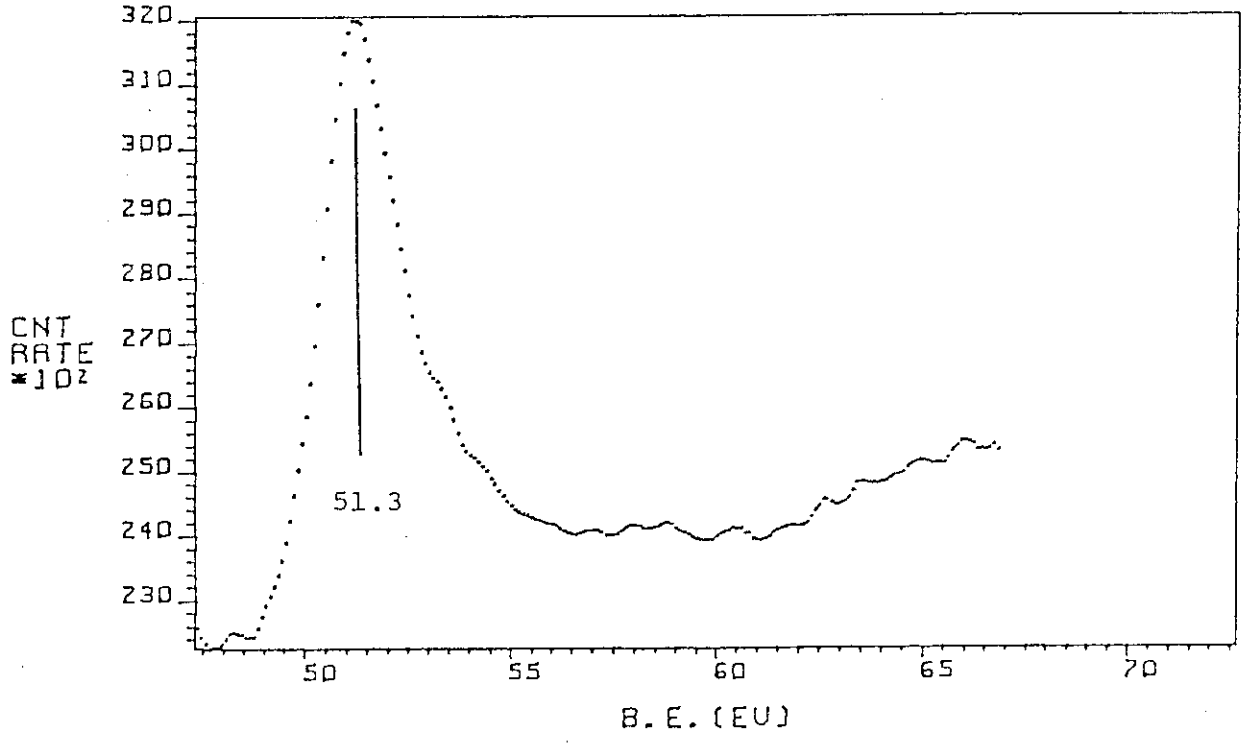

Fig. 4 Sc3s XPS spectrum of Sc_{fl}.

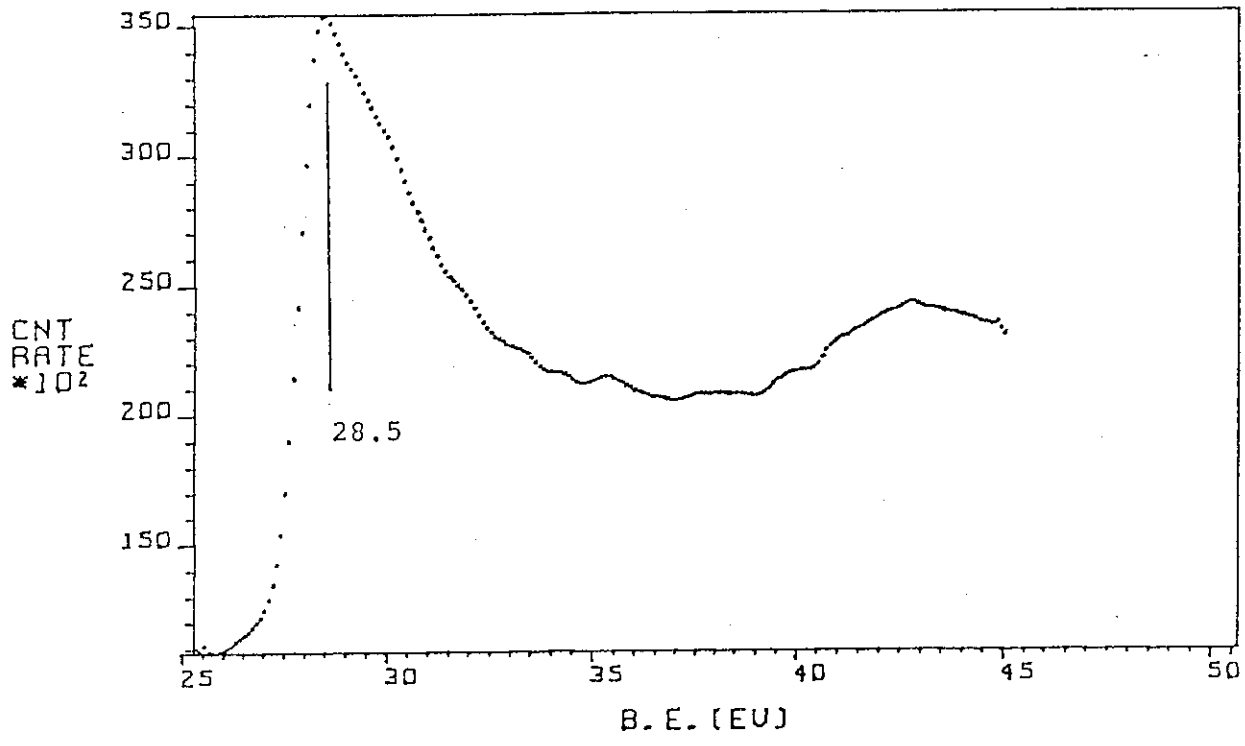

Fig. 5 Sc3p XPS spectrum of Sc_{fl}.

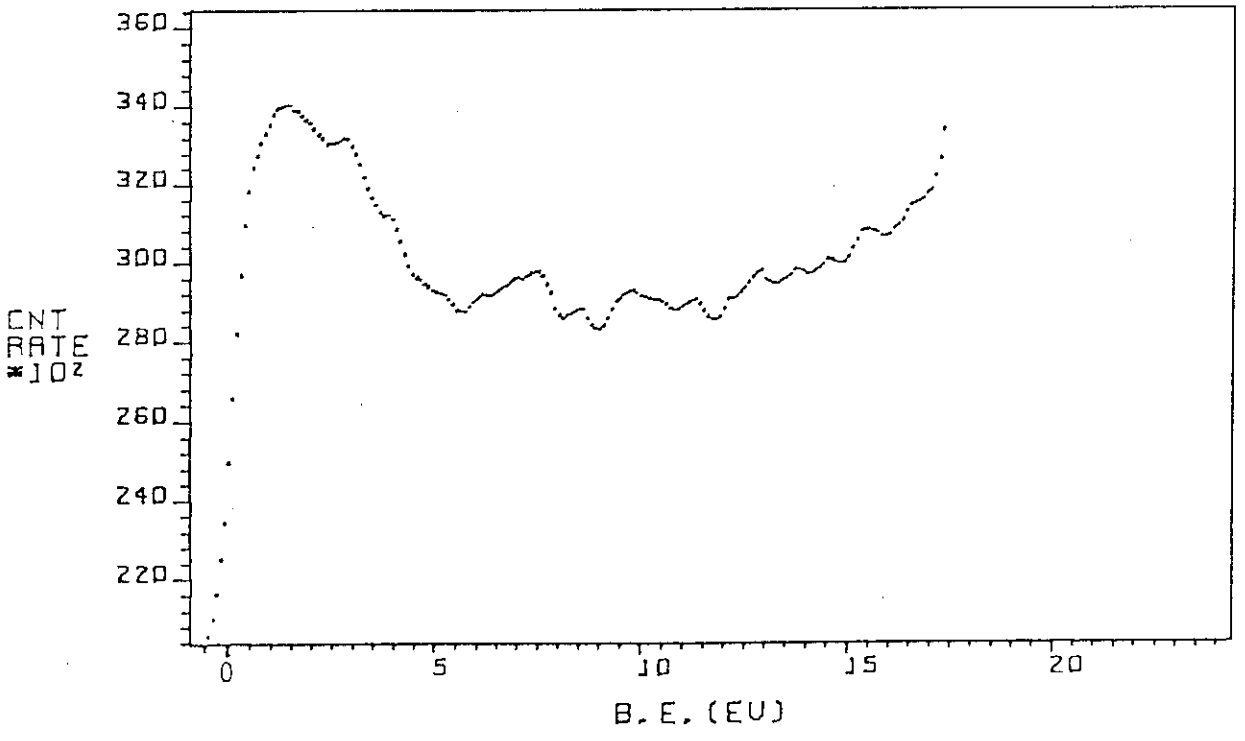

Fig. 6 Valence-band spectrum of Sc_{fl}.

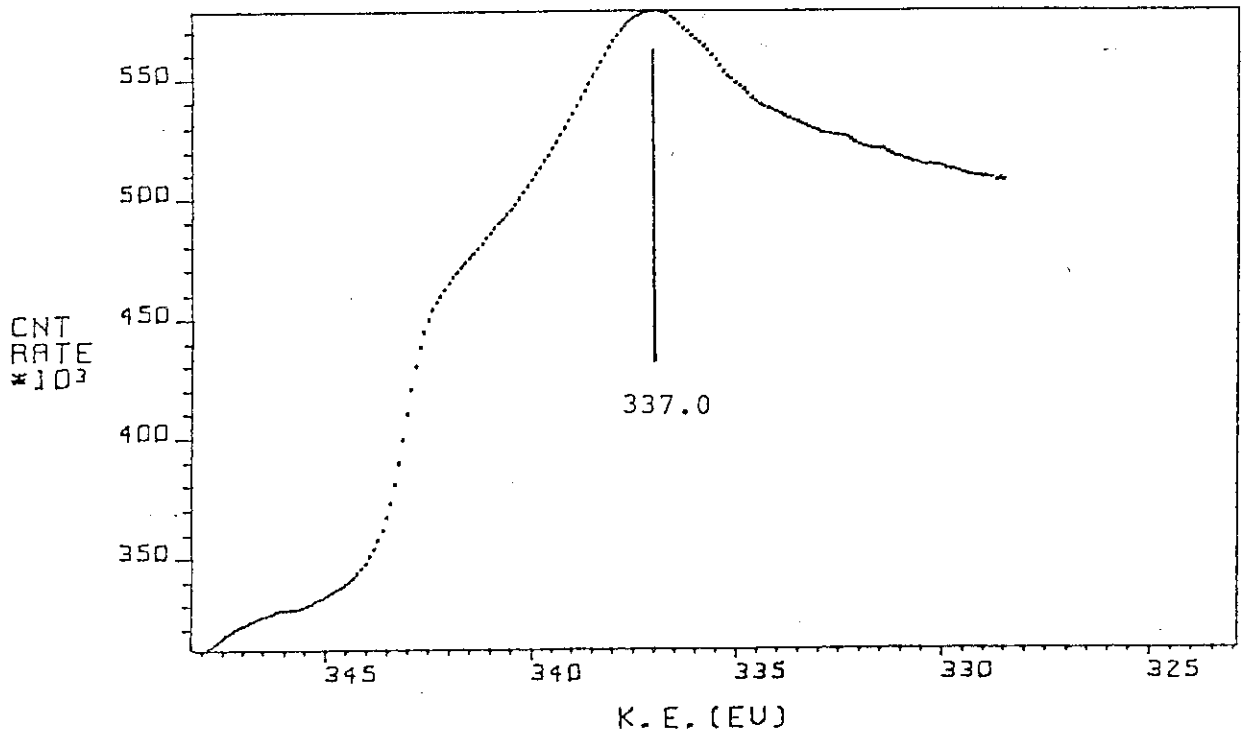

Fig. 7 $L_{2,3}M_{2,3}M_{2,3}$ XAES spectrum of Sc_{fl}.

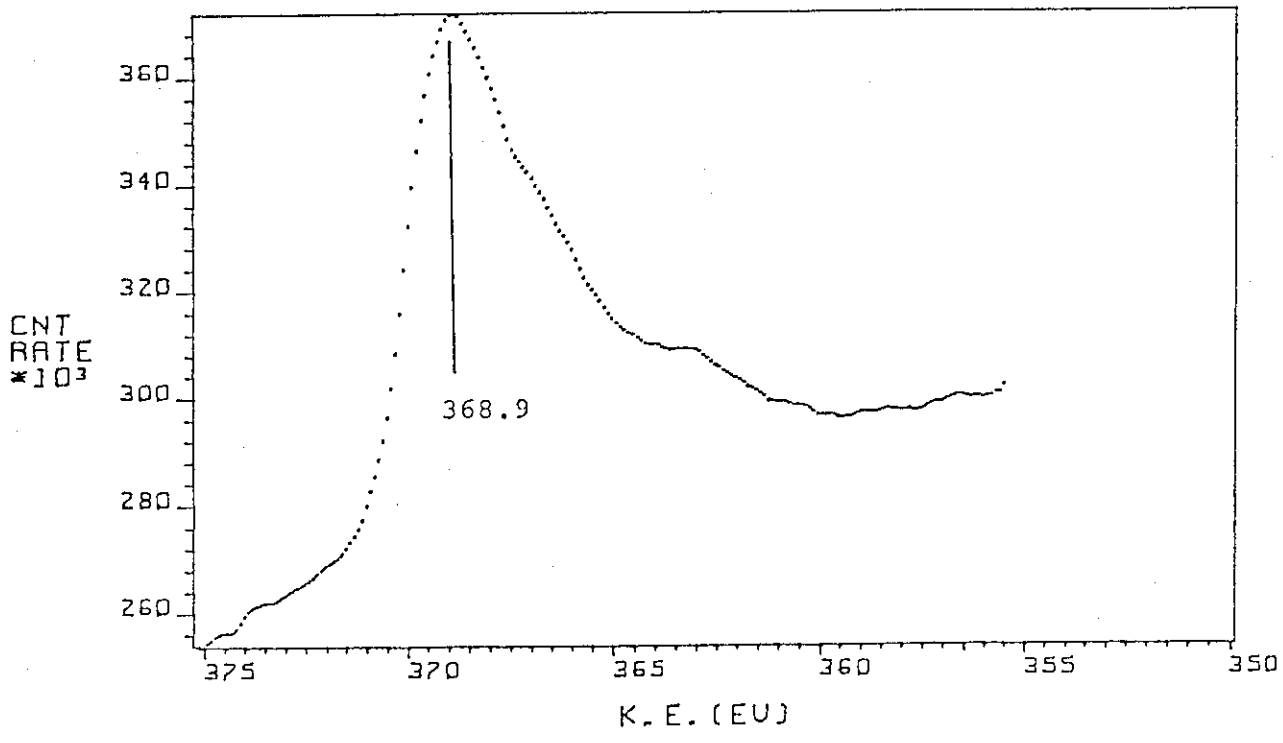

Fig. 8 $L_{2,3}M_{2,3}V$ XAES spectrum of Sc_{fl}.

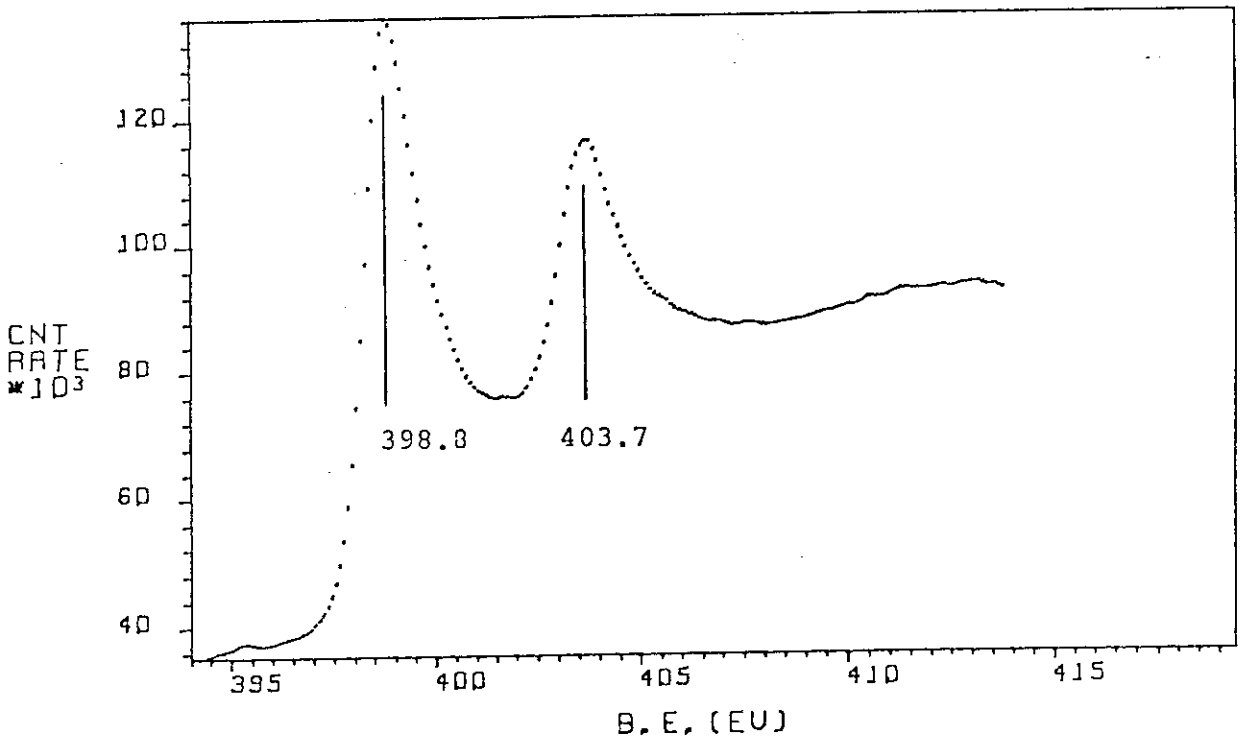

Fig. 9 Sc2p XPS spectrum of Sc_{et}.

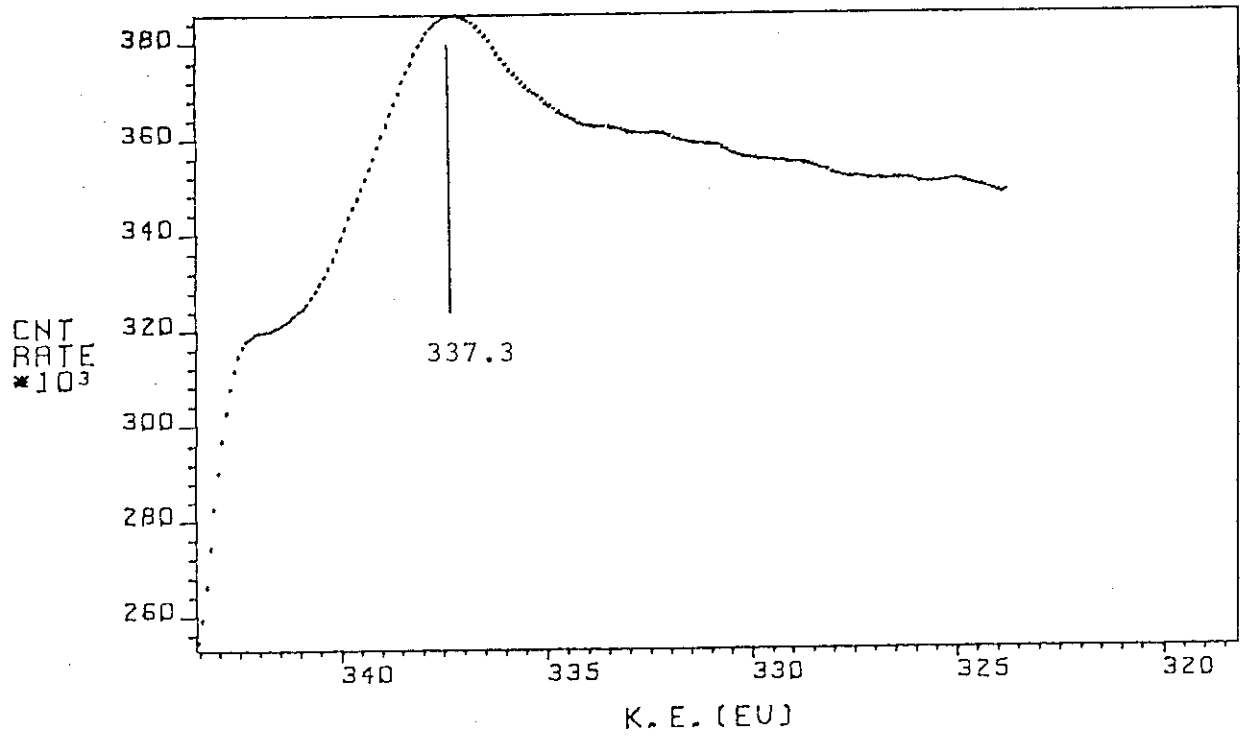

Fig. 10 $L_{2,3}M_{2,3}M_{2,3}$ XAES spectrum of Sc_{et}.

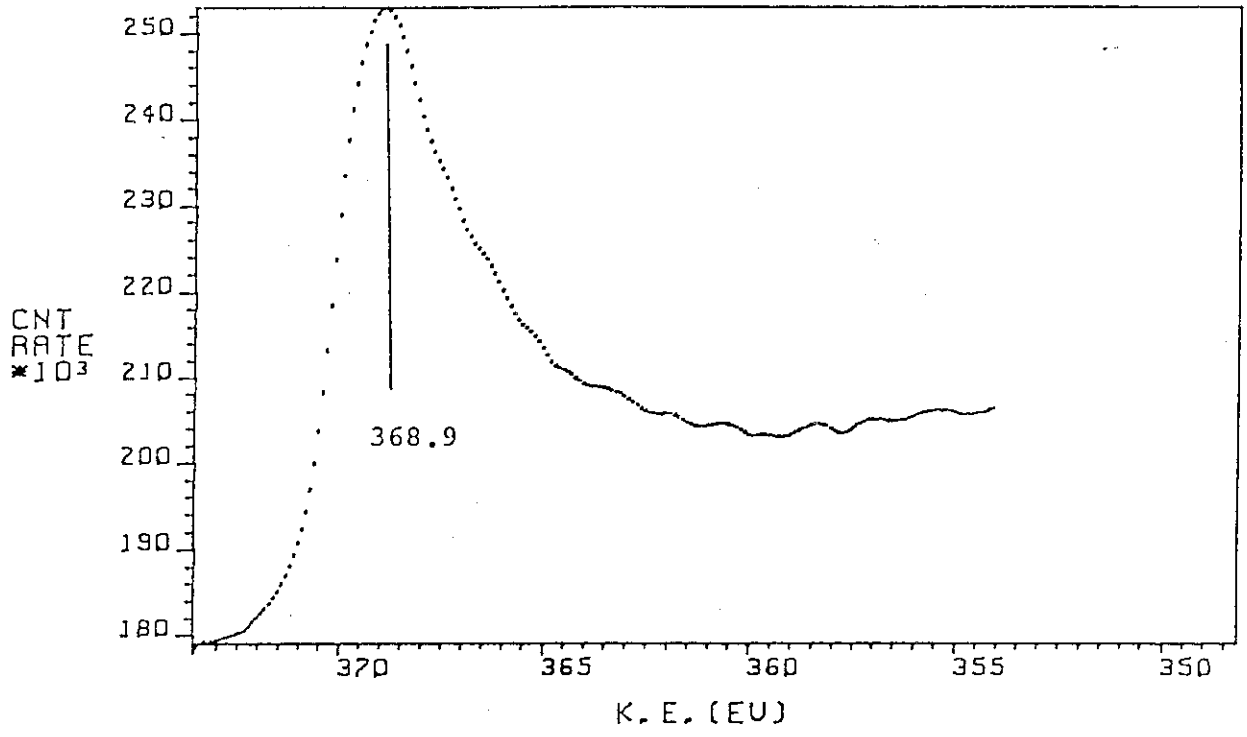

Fig. 11 $L_{2,3}M_{2,3}V$ XAES spectrum of Sc_{et}.

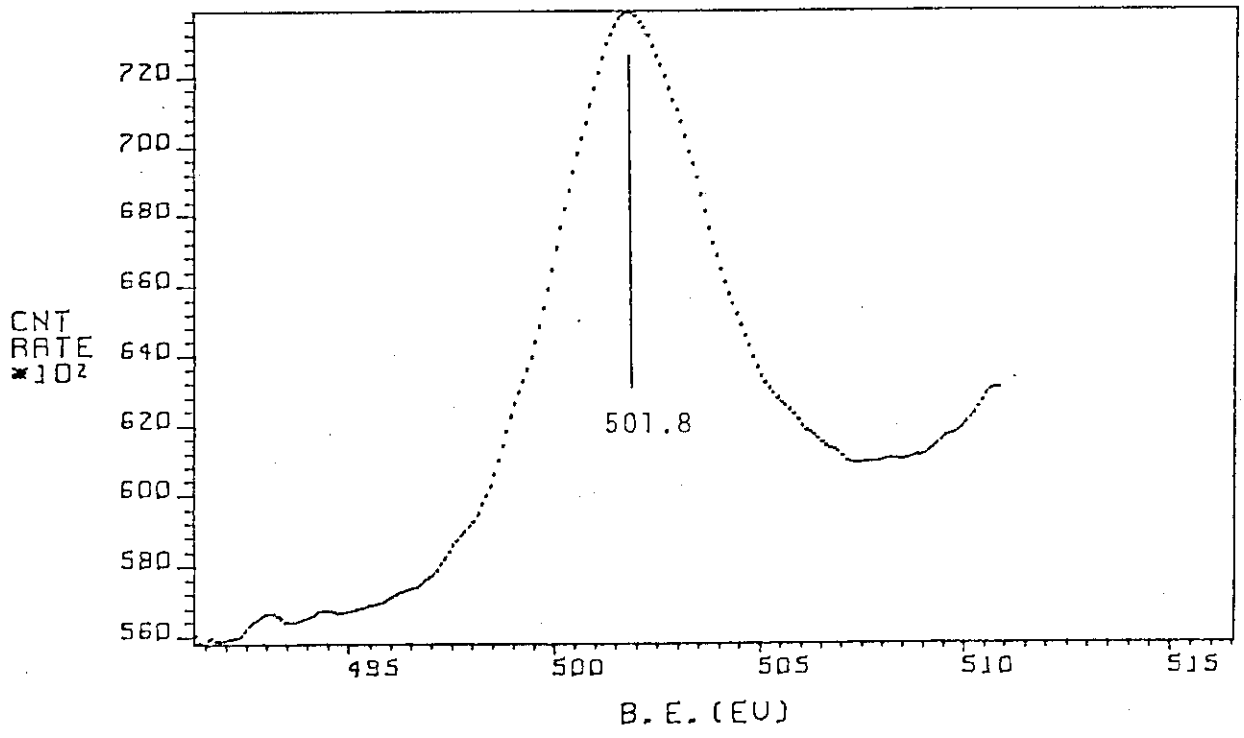

Fig. 12 Sc2s XPS spectrum of Sc_2O_3.

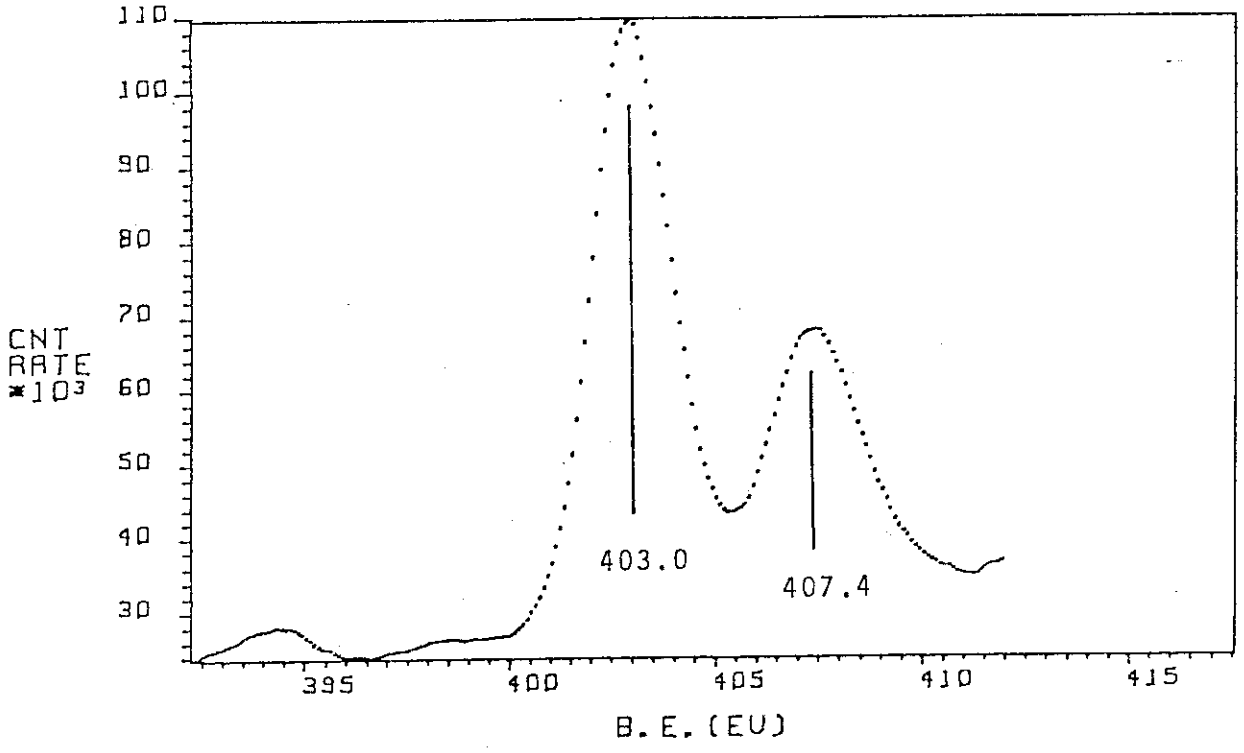

Fig. 13 Sc2p XPS spectrum of Sc_2O_3.

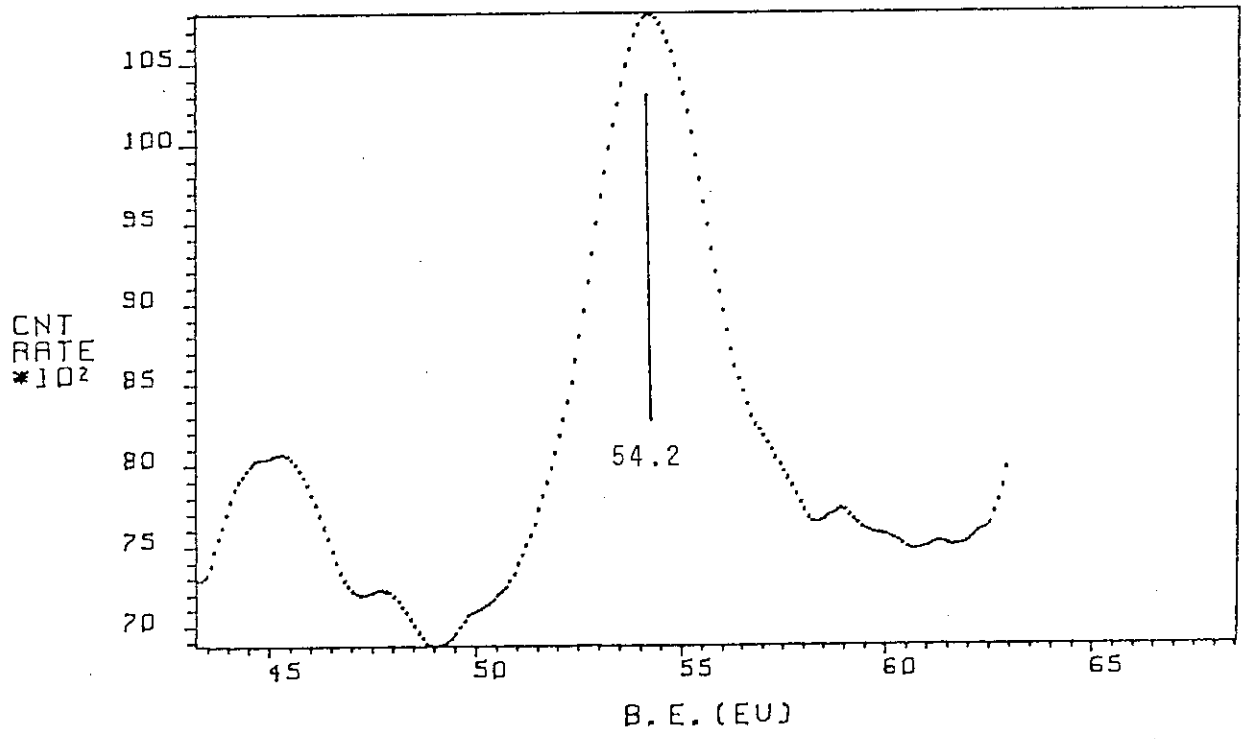

Fig. 14 Sc3s XPS spectrum of Sc_2O_3.

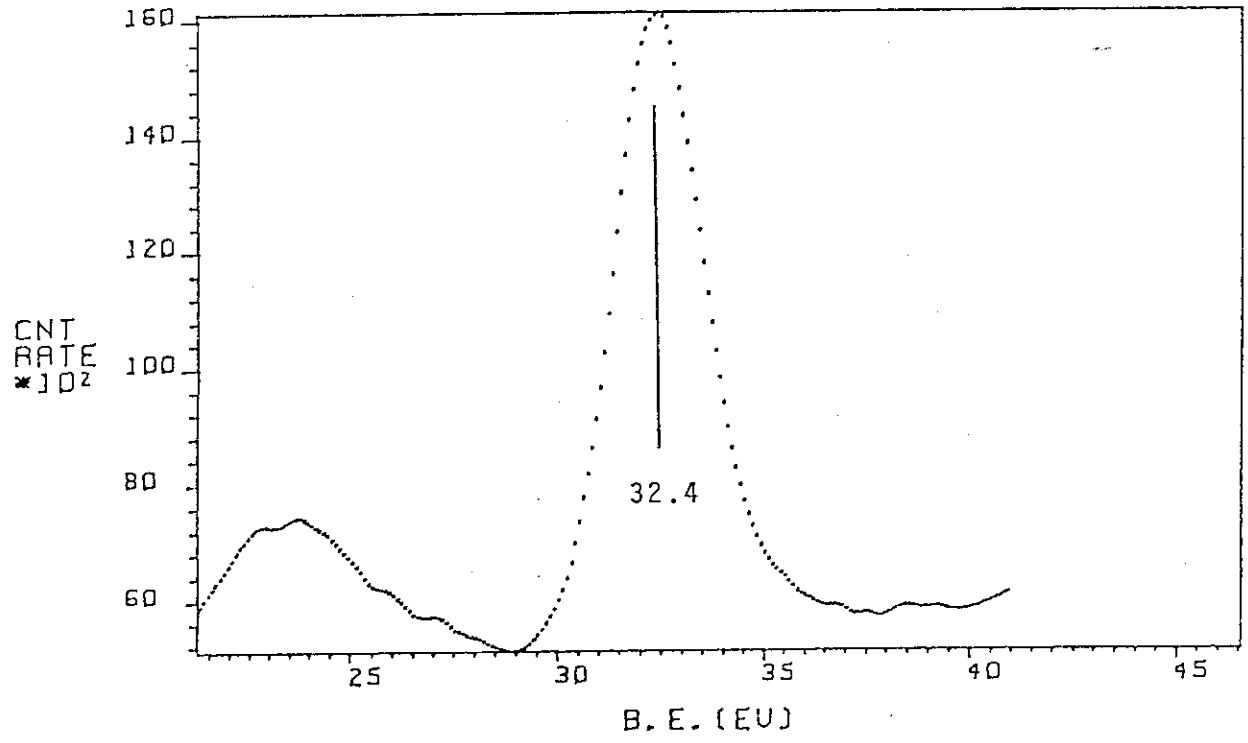

Fig. 15 Sc3p XPS spectrum of Sc_2O_3.

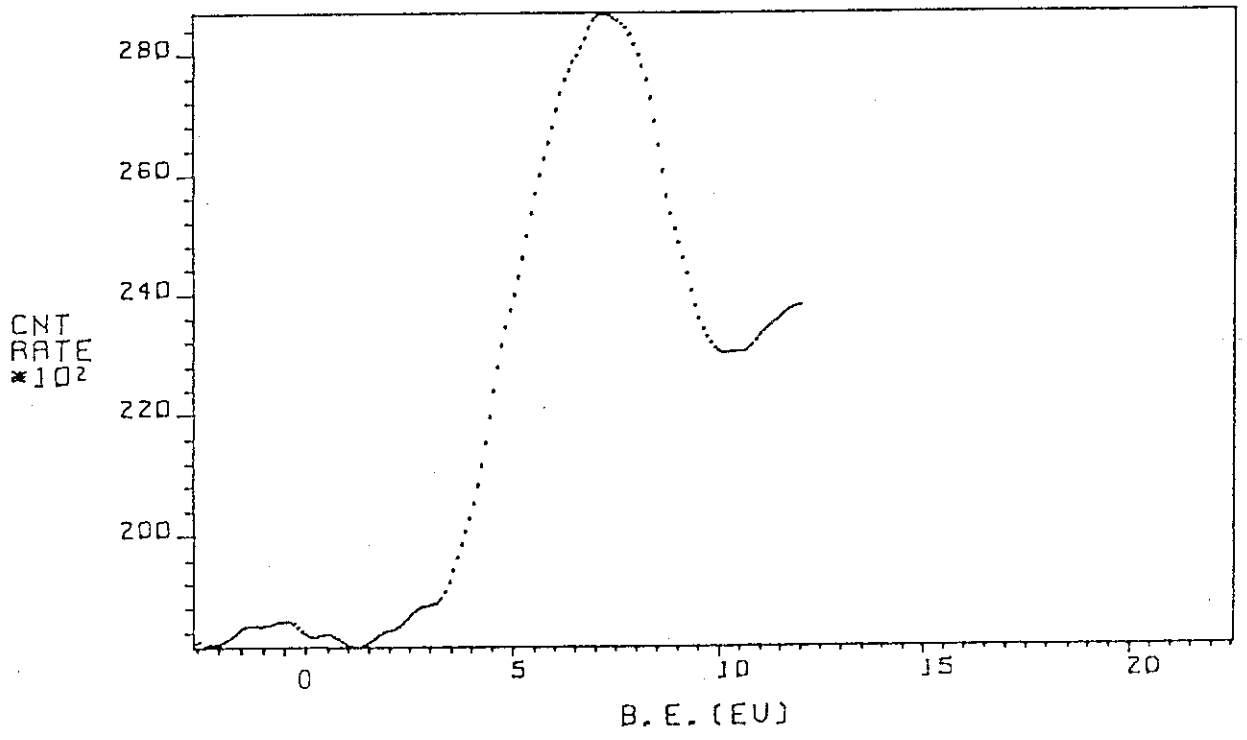

Fig. 16 Valence-band spectrum of Sc_2O_3.

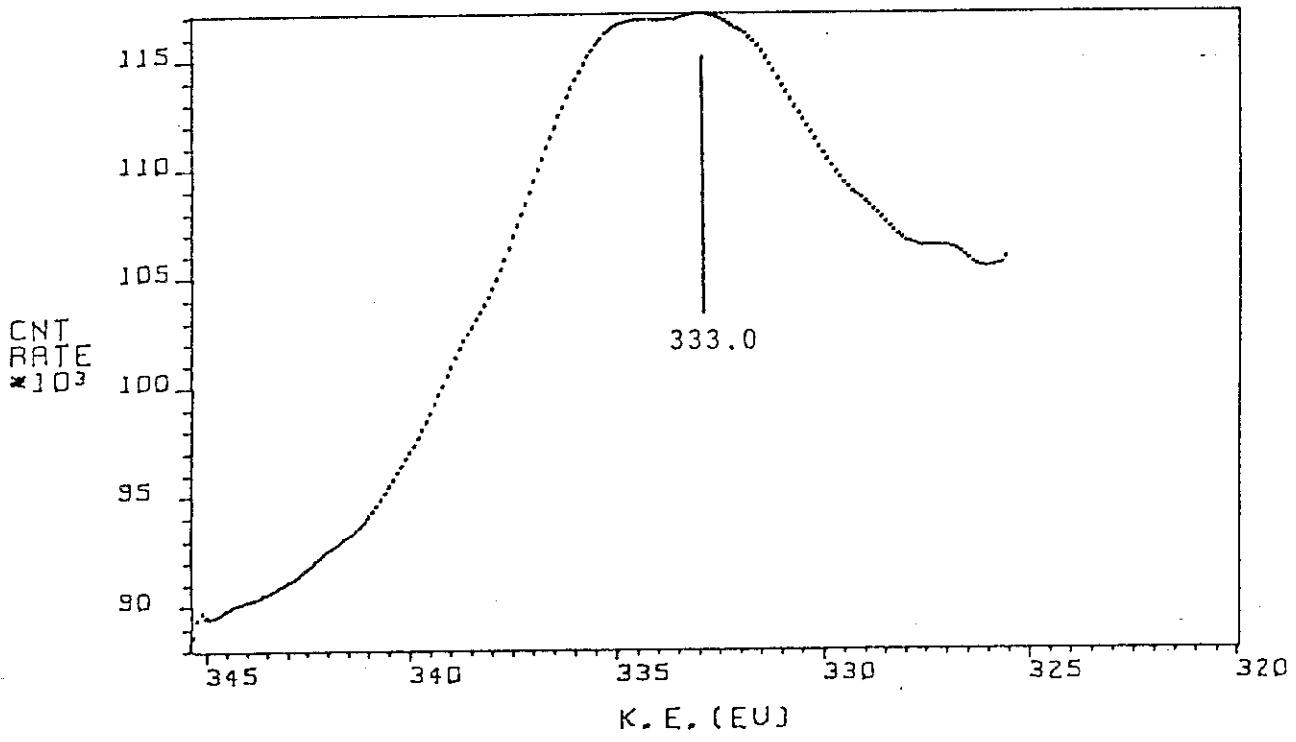

Fig. 17 $L_{2,3}M_{2,3}M_{2,3}$ XAES spectrum of Sc_2O_3.

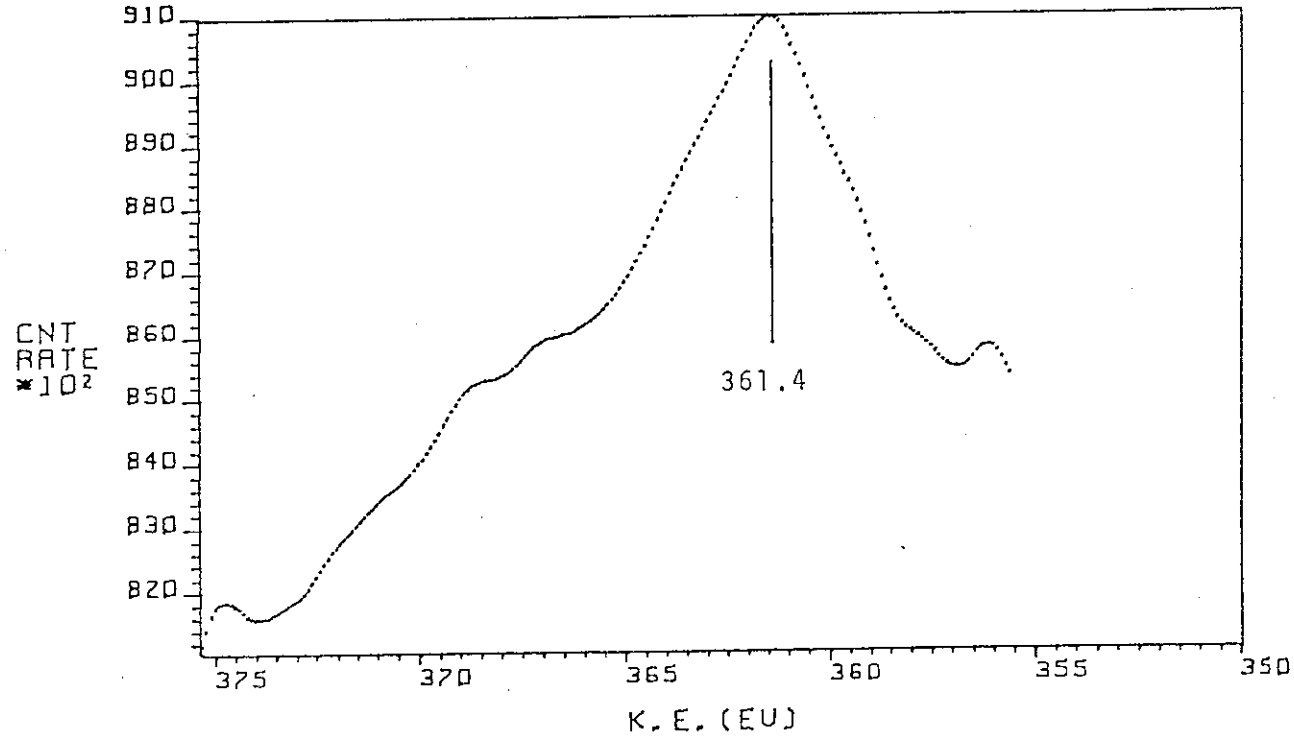

Fig. 18 $L_{2,3}M_{2,3}V$ XAES spectrum of Sc_2O_3.

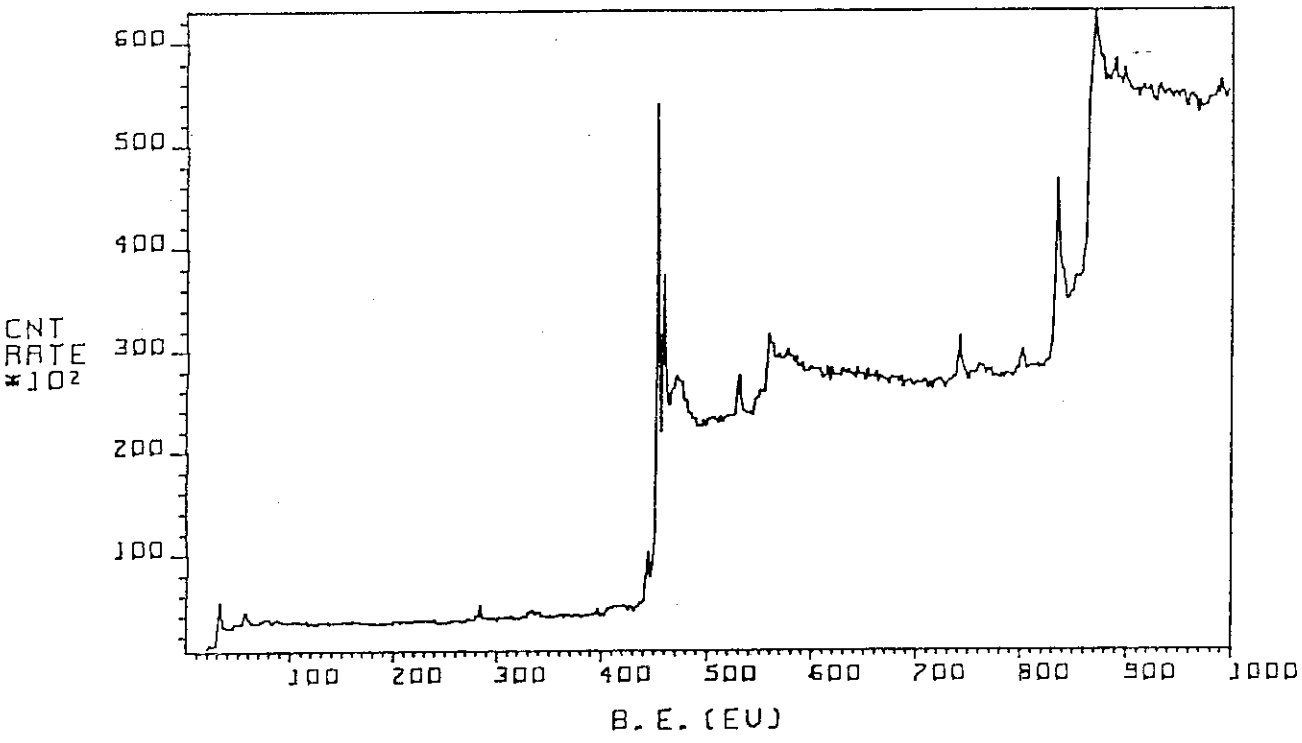

Fig. 19 XPS wide scan of Ti_{fl}.

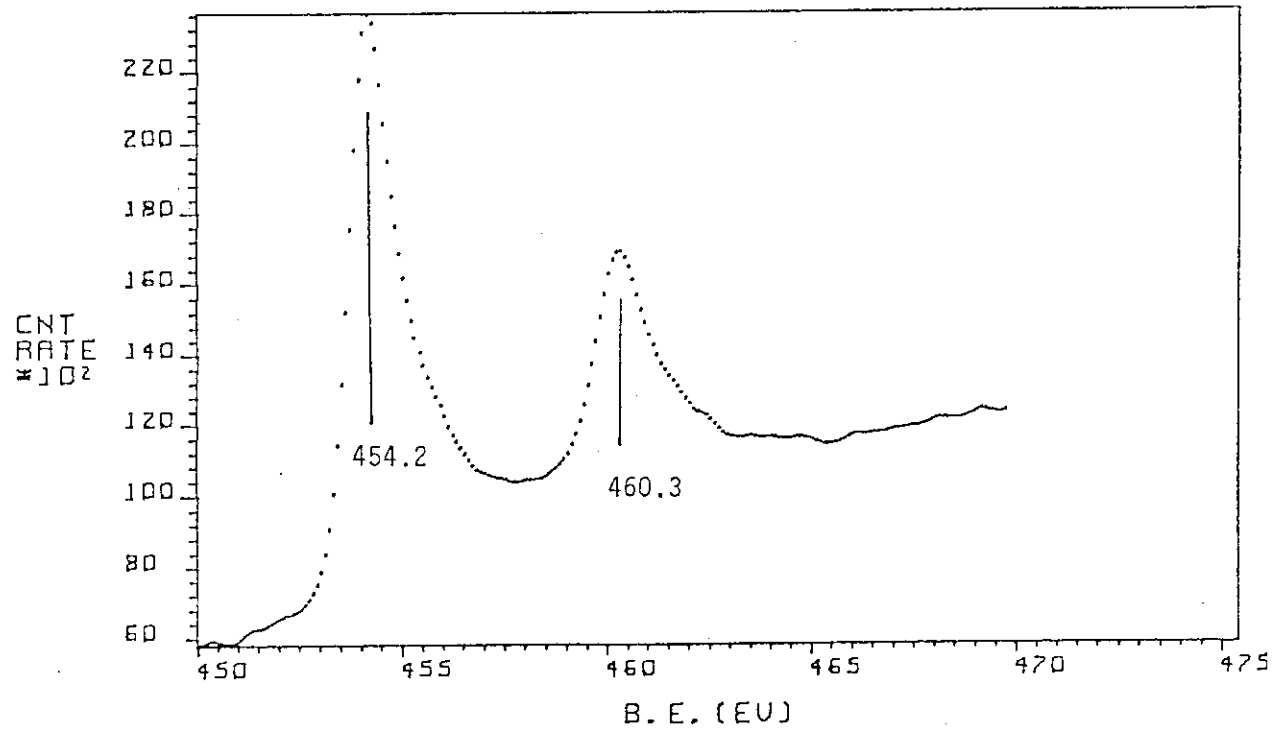

Fig. 20 Ti2p XPS spectrum of Ti_{fl}.

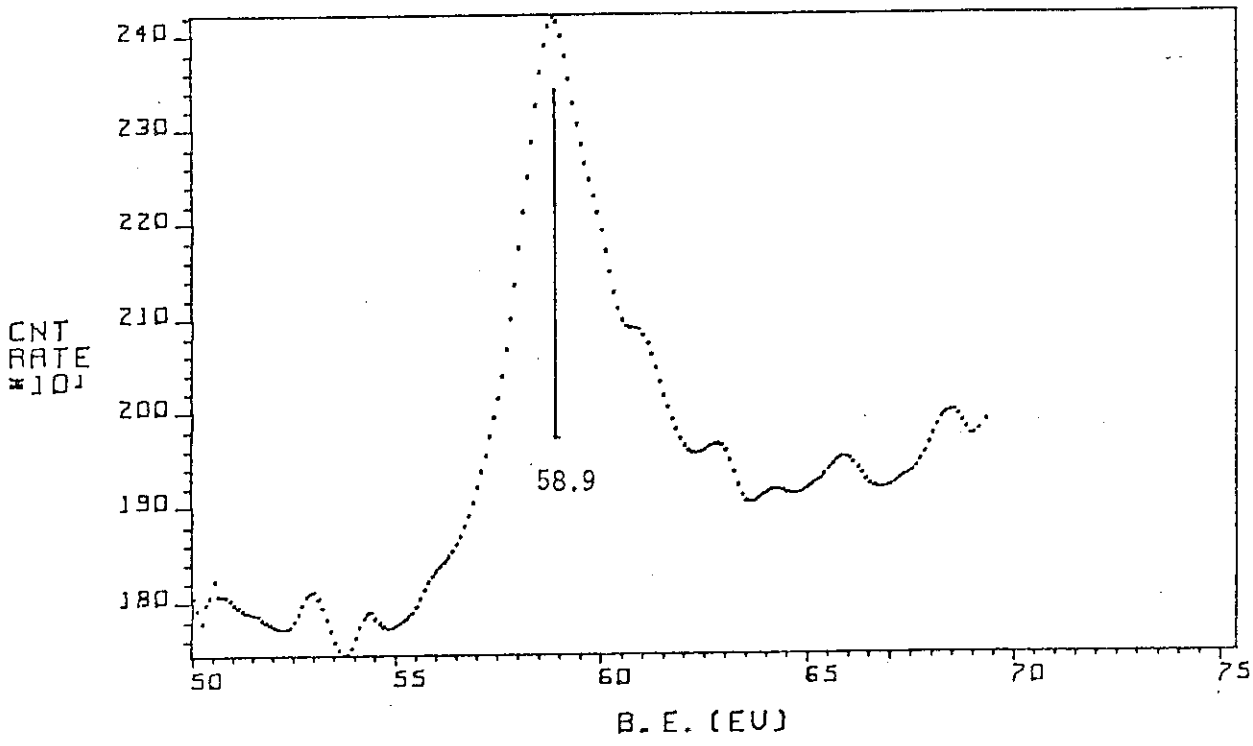

Fig. 21 Ti3s XPS spectrum of Ti_{fl}.

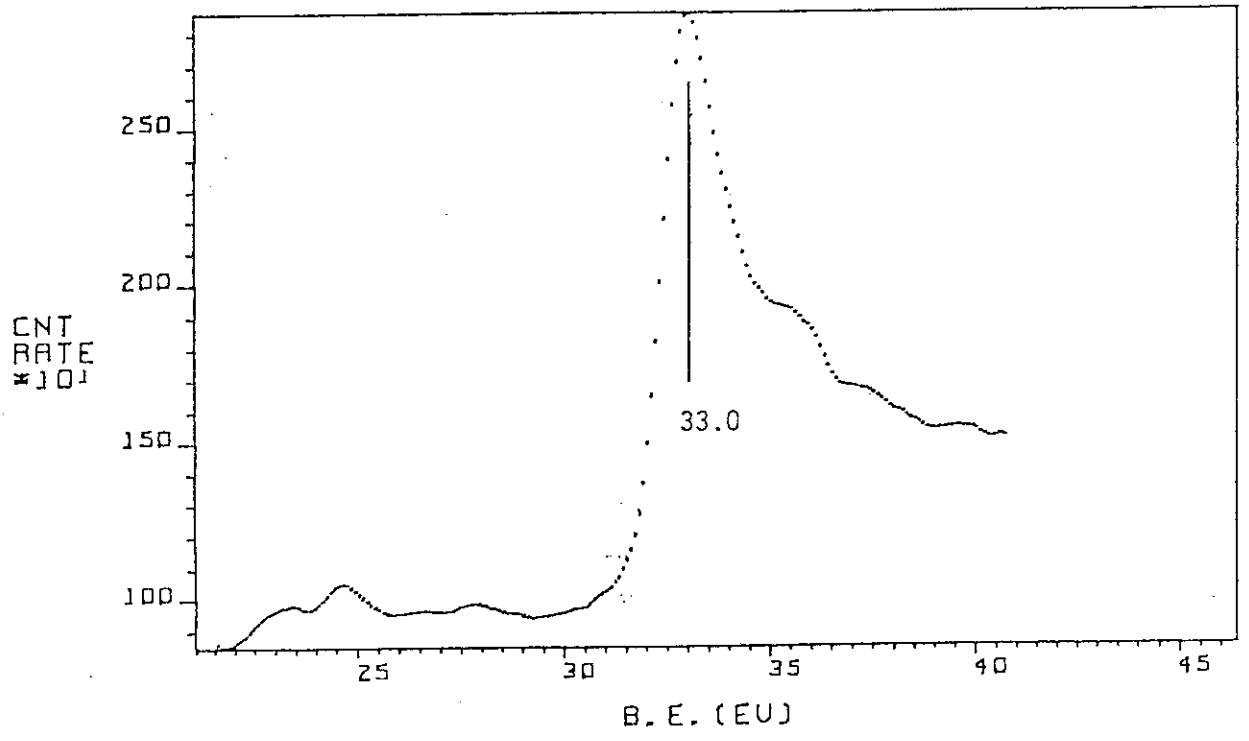

Fig. 22 Ti3p XPS spectrum of Ti_{fl}.

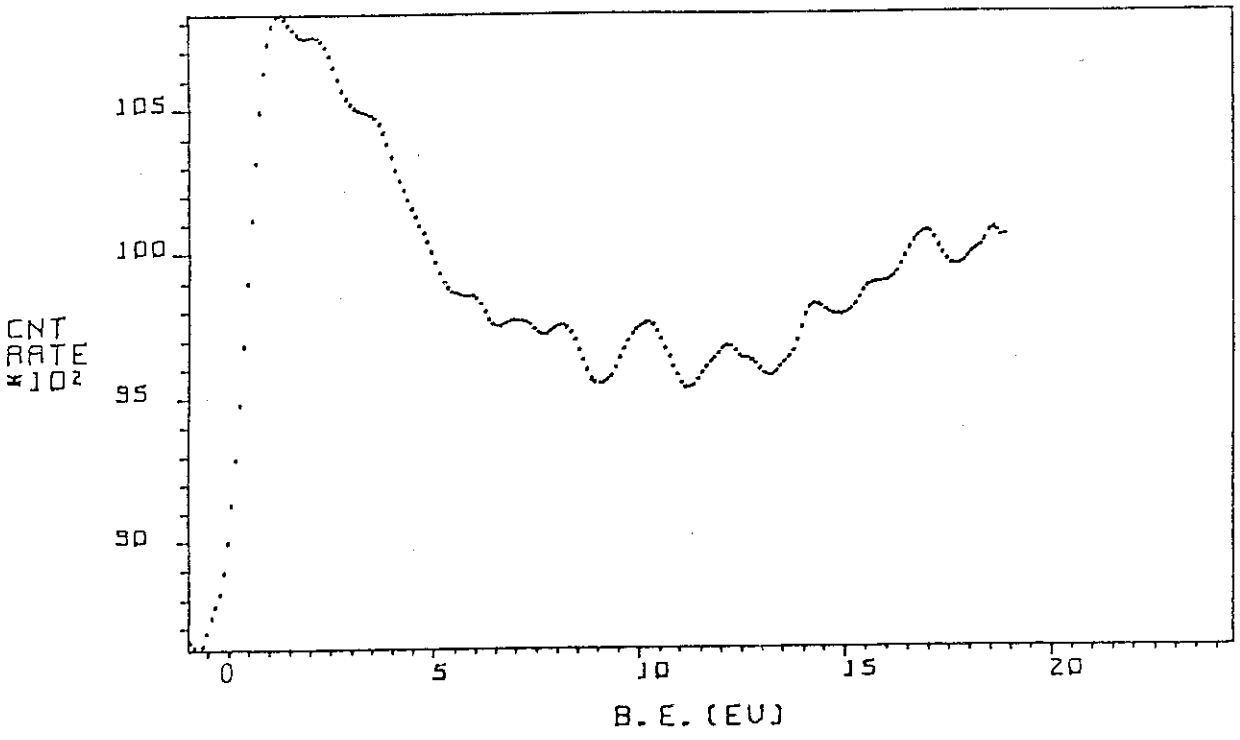

Fig. 23 Valence-band spectrum of Ti_{fl}.

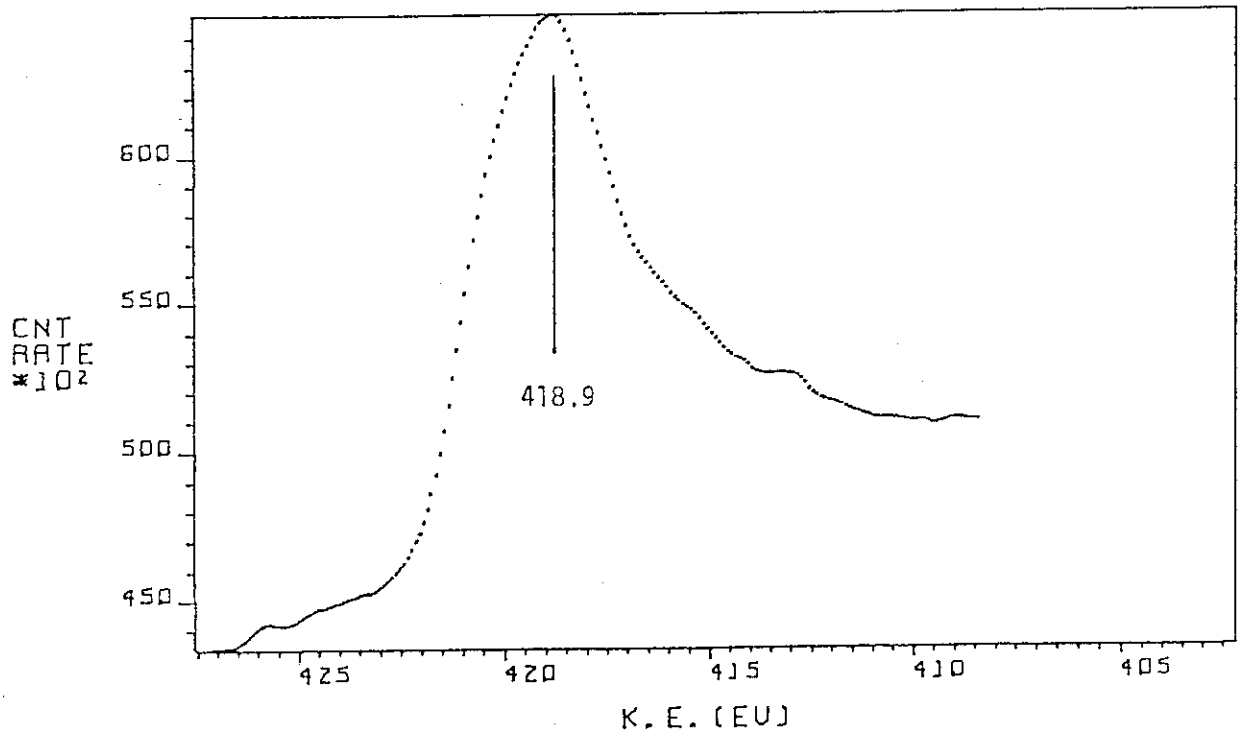

Fig. 24 $L_3M_{2,3}V$ XAES spectrum of Ti_{fl}.

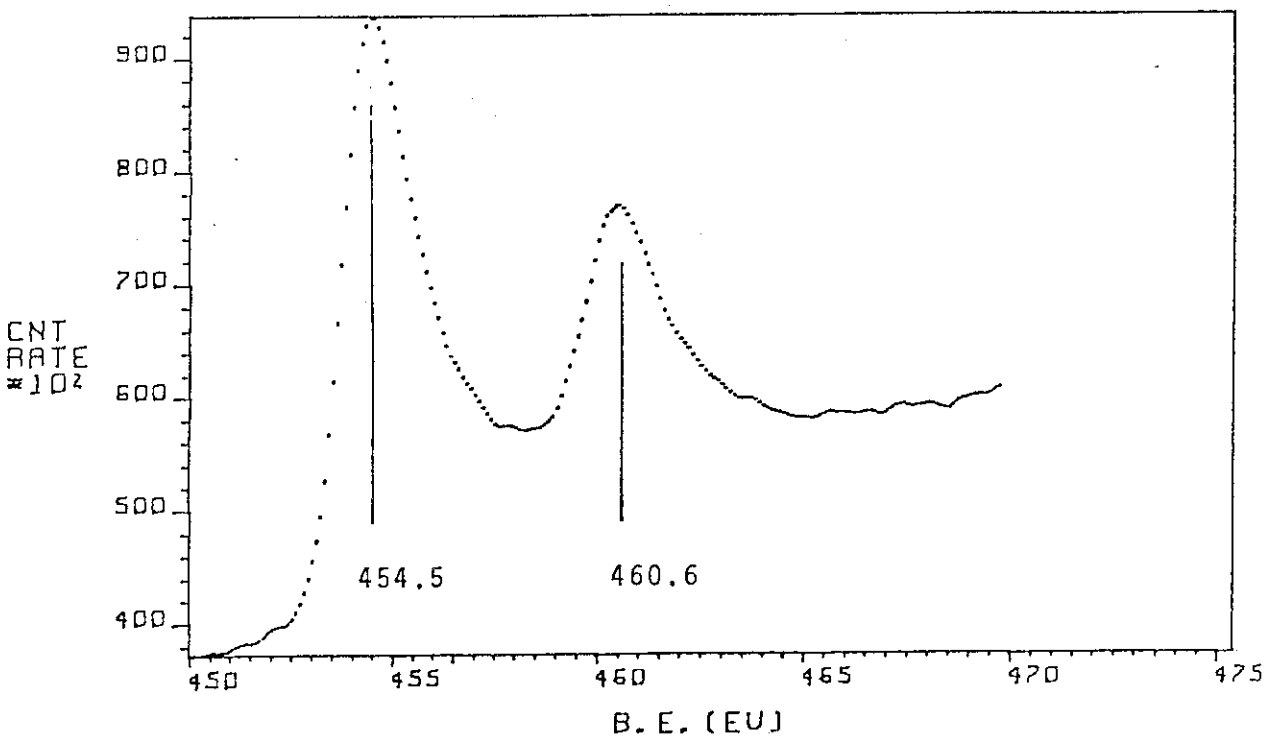

Fig. 25 Ti2p XPS spectrum of Ti_{et}.

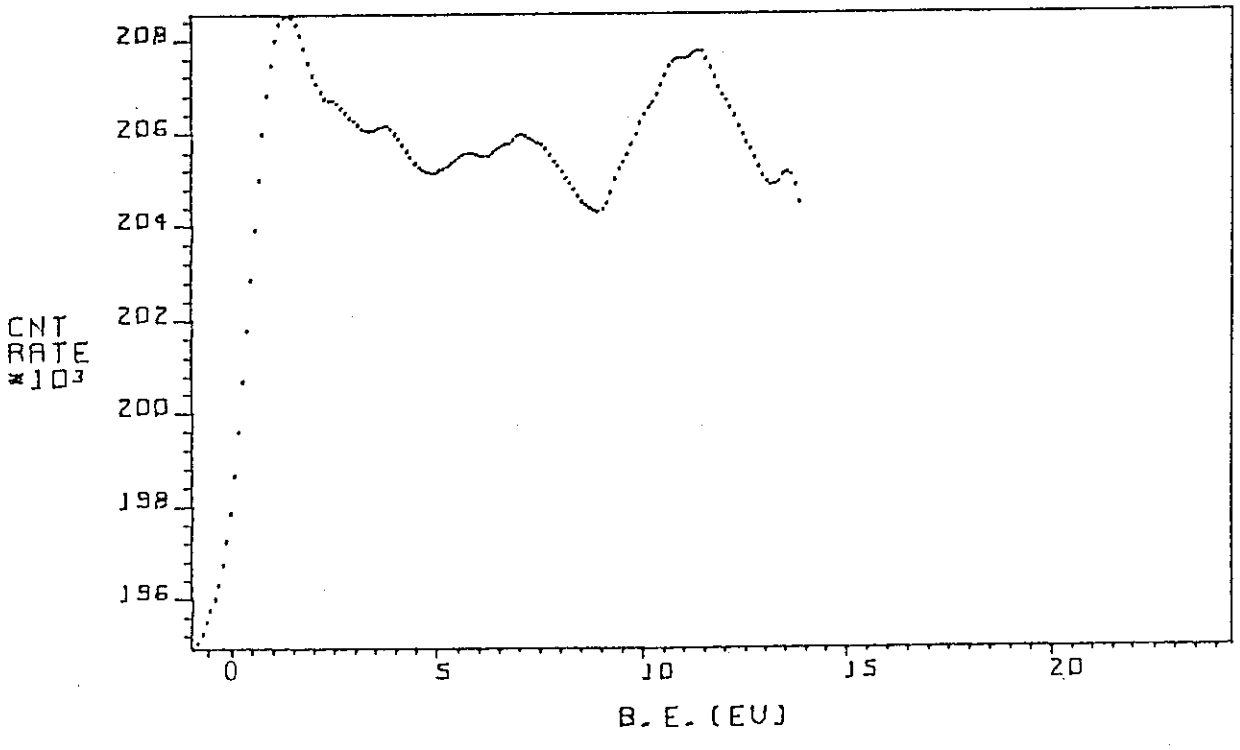

Fig. 26 Valence-band spectrum of Ti_{et}.

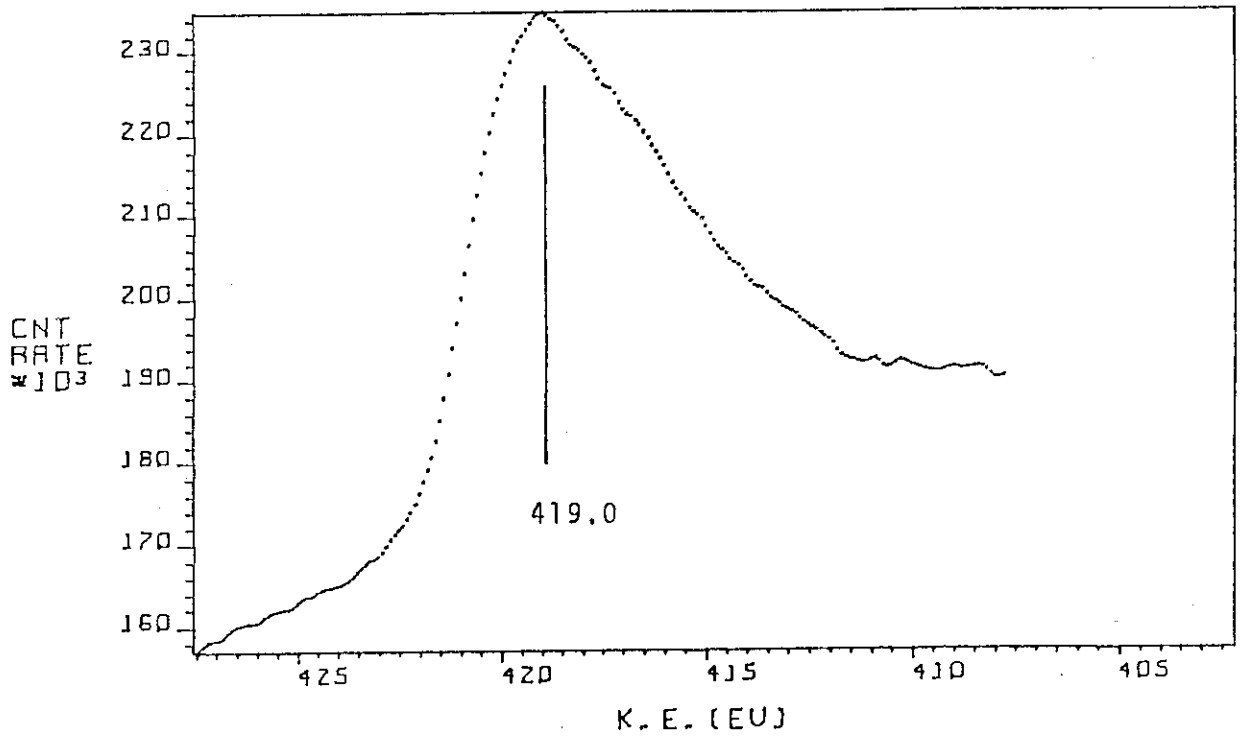

Fig. 27 $L_3M_{2,3}V$ XAES spectrum of Ti_{et}.

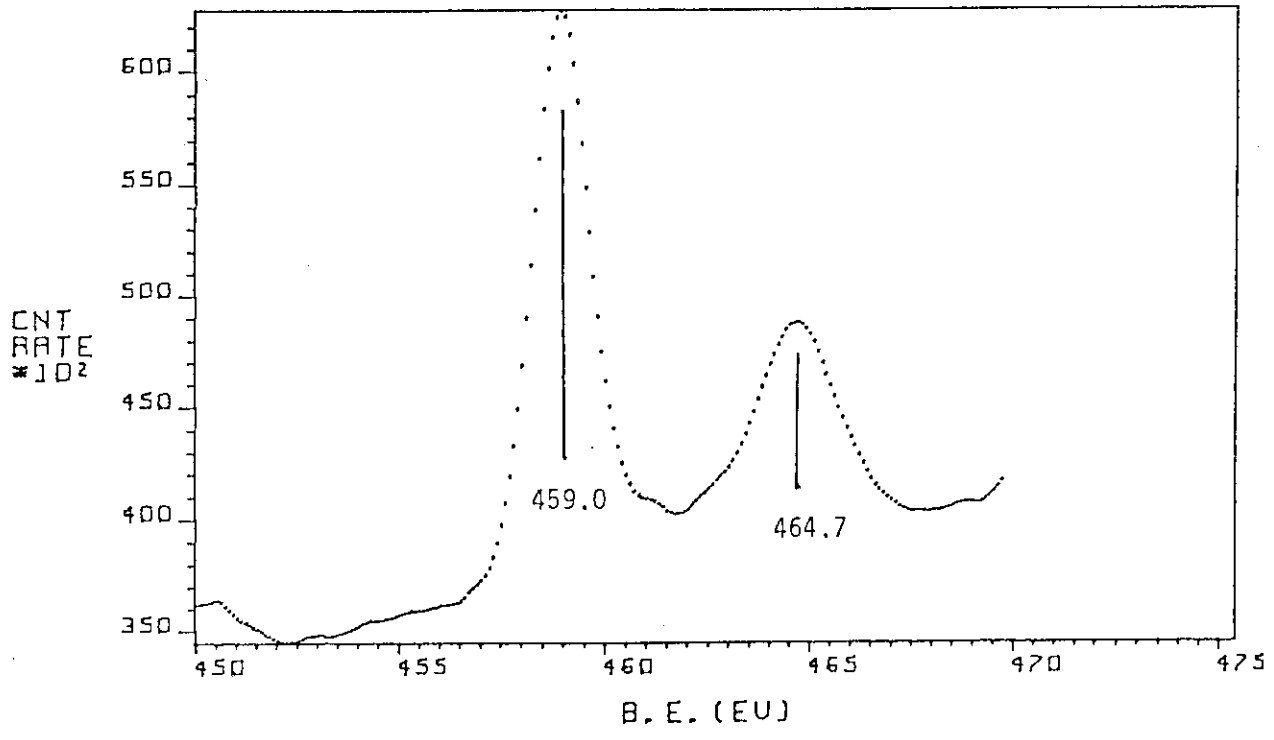

Fig. 28 Ti2p XPS spectrum of TiO_2.

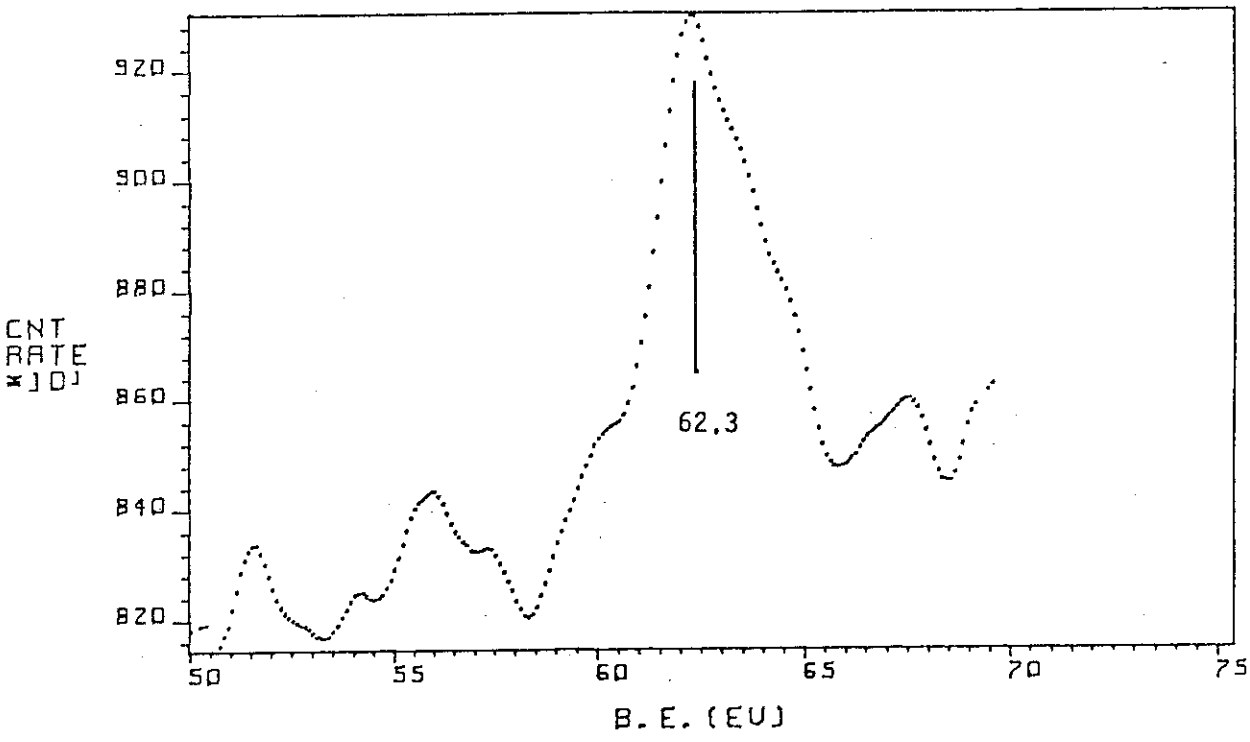

Fig. 29 Ti3s XPS spectrum of TiO_2.

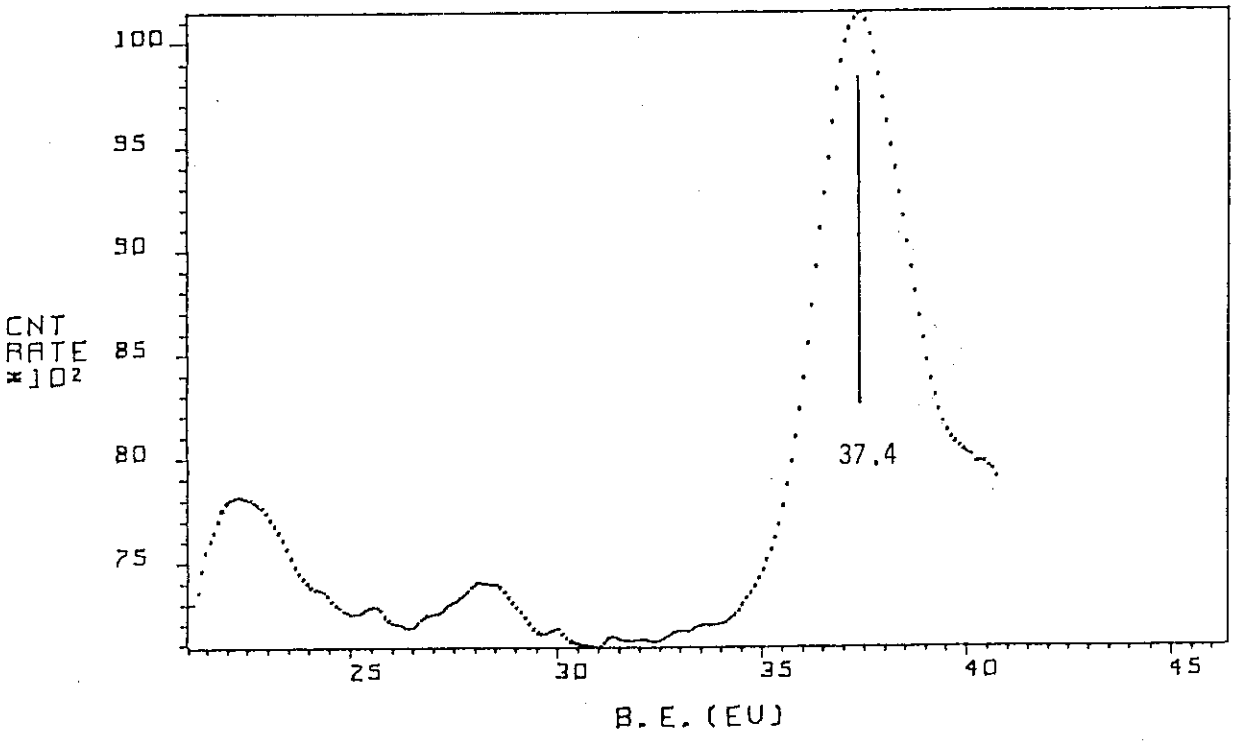

Fig. 30 Ti3p XPS spectrum of TiO_2.

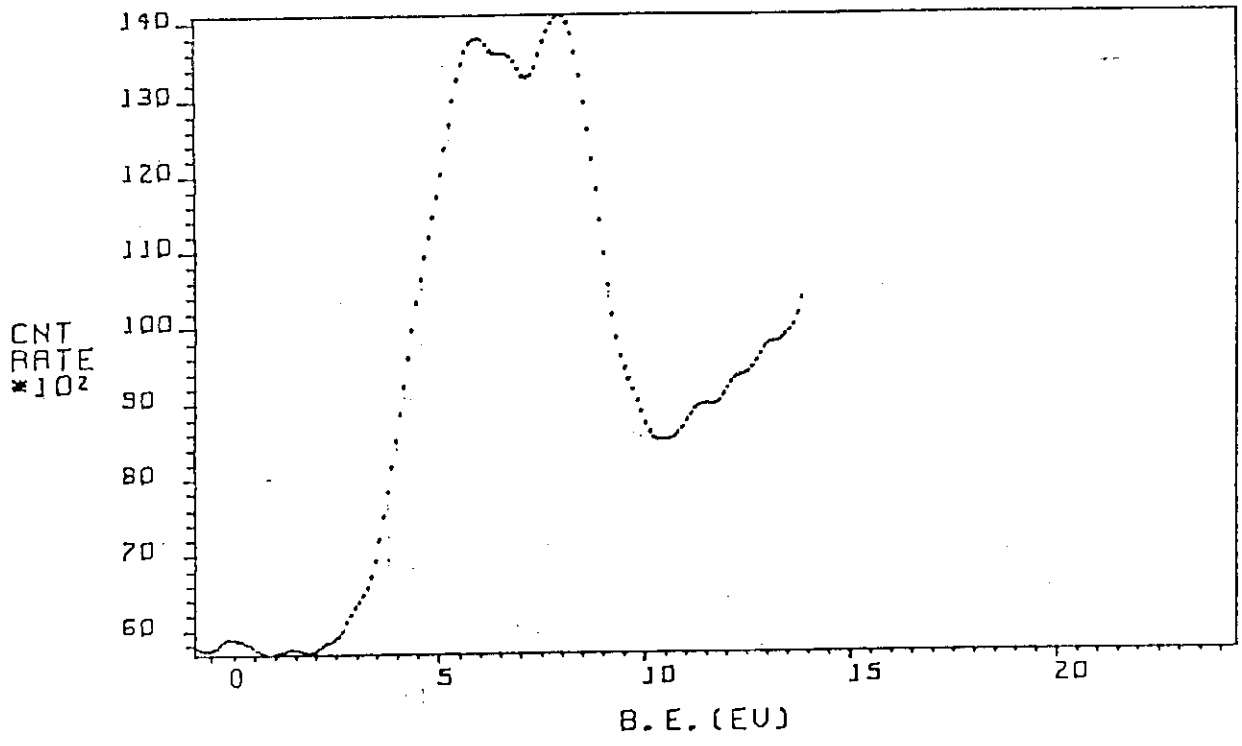

Fig. 31 Valence-band spectrum of TiO_2.

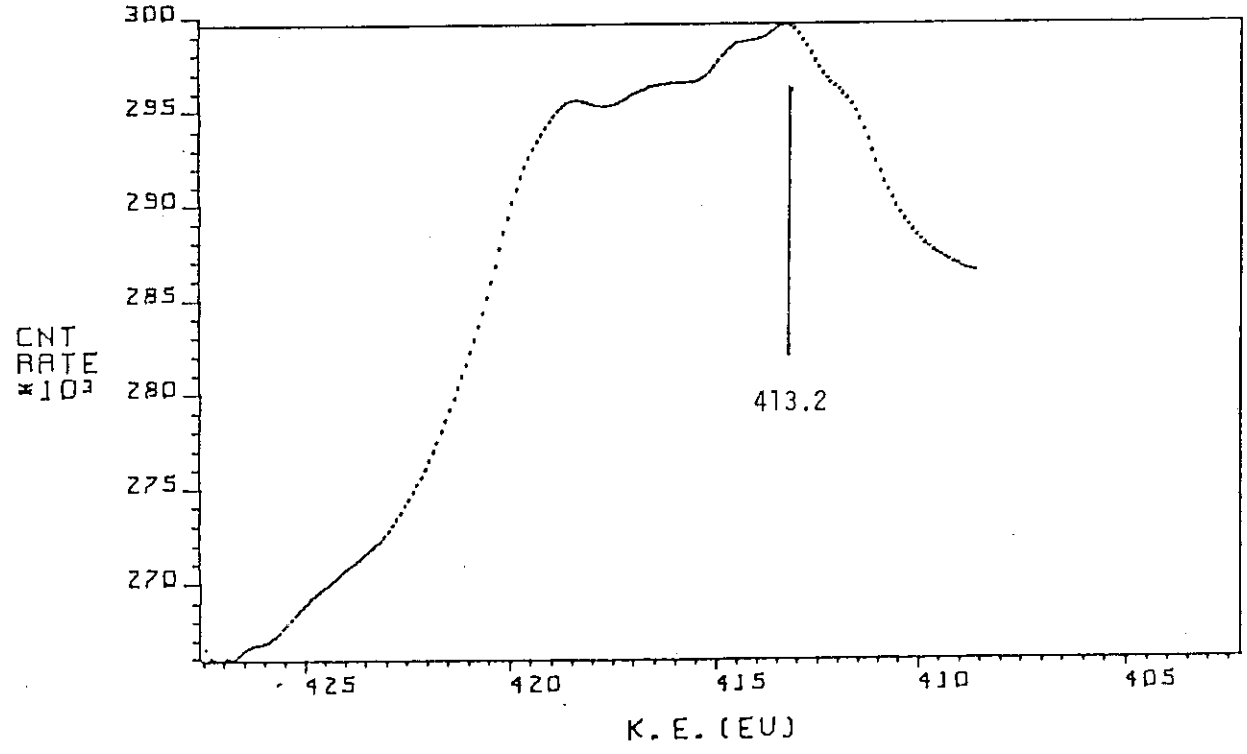

Fig. 32 $L_3M_{2,3}V$ XAES spectrum of TiO_2.

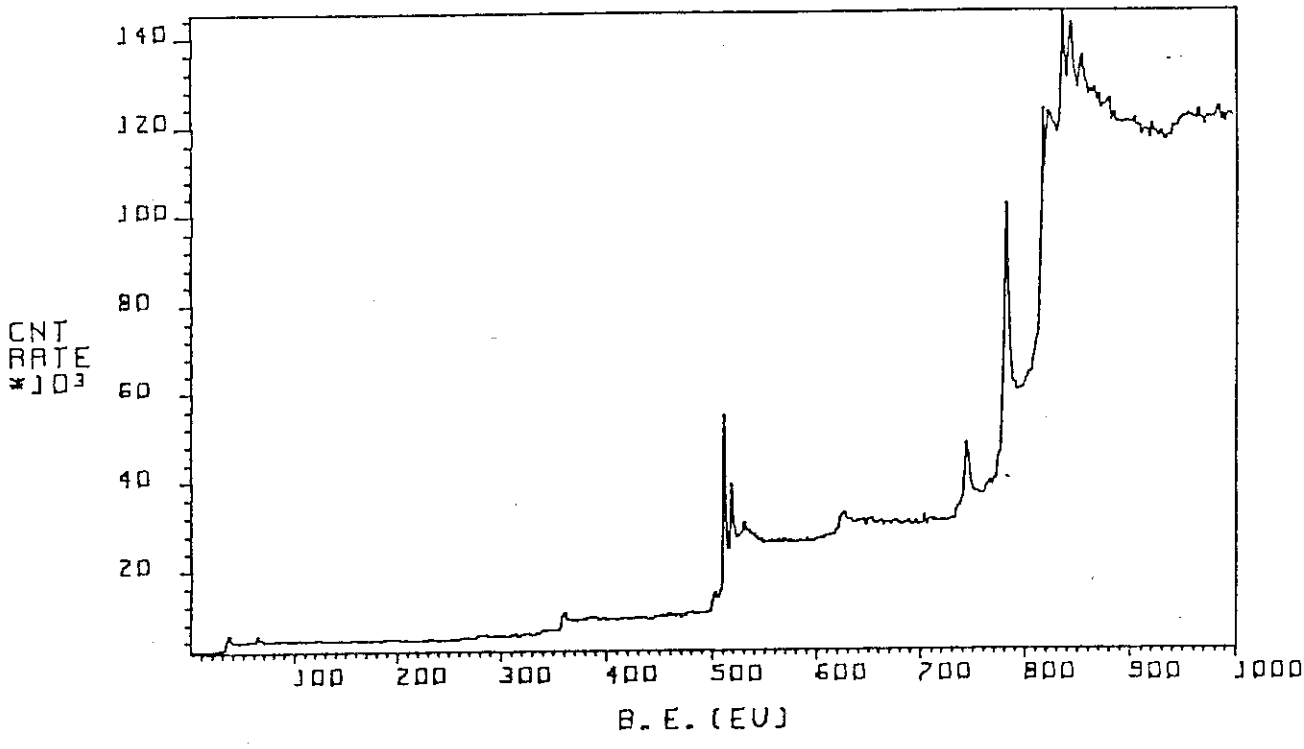

Fig. 33 XPS wide scan of V_{fl}.

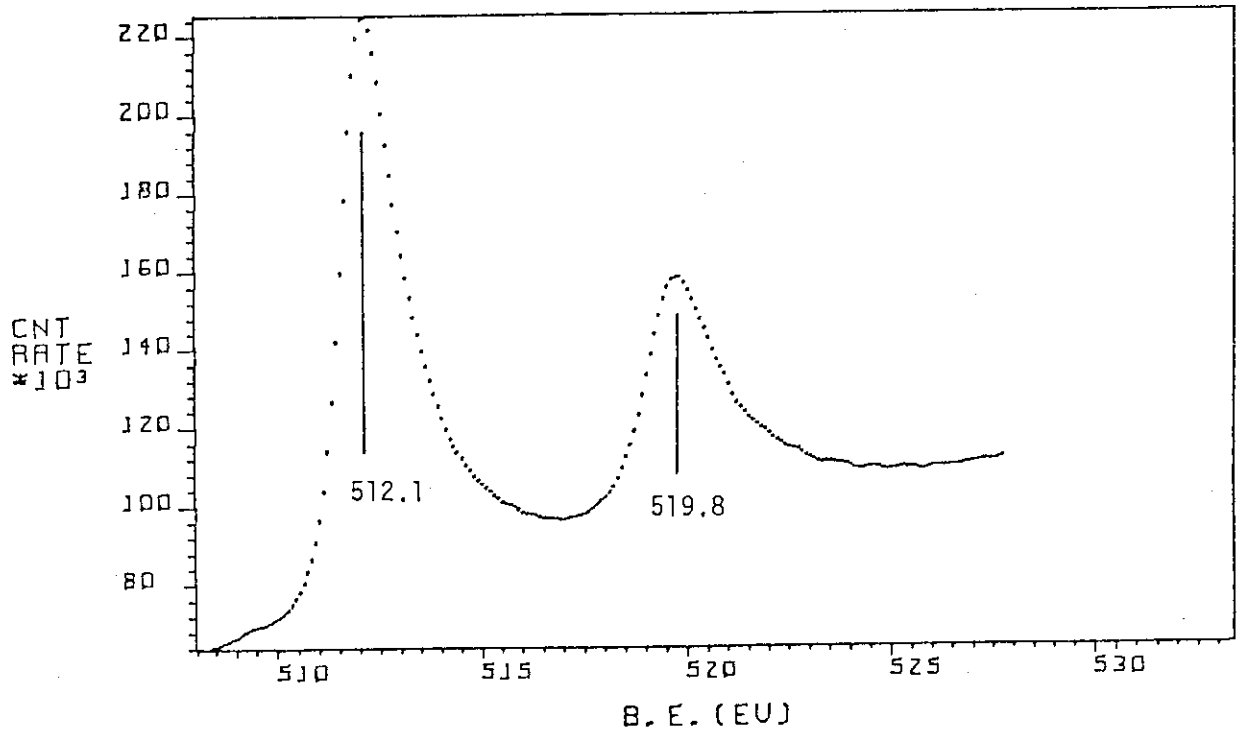

Fig. 34 V2p XPS spectrum of V_{fl}.

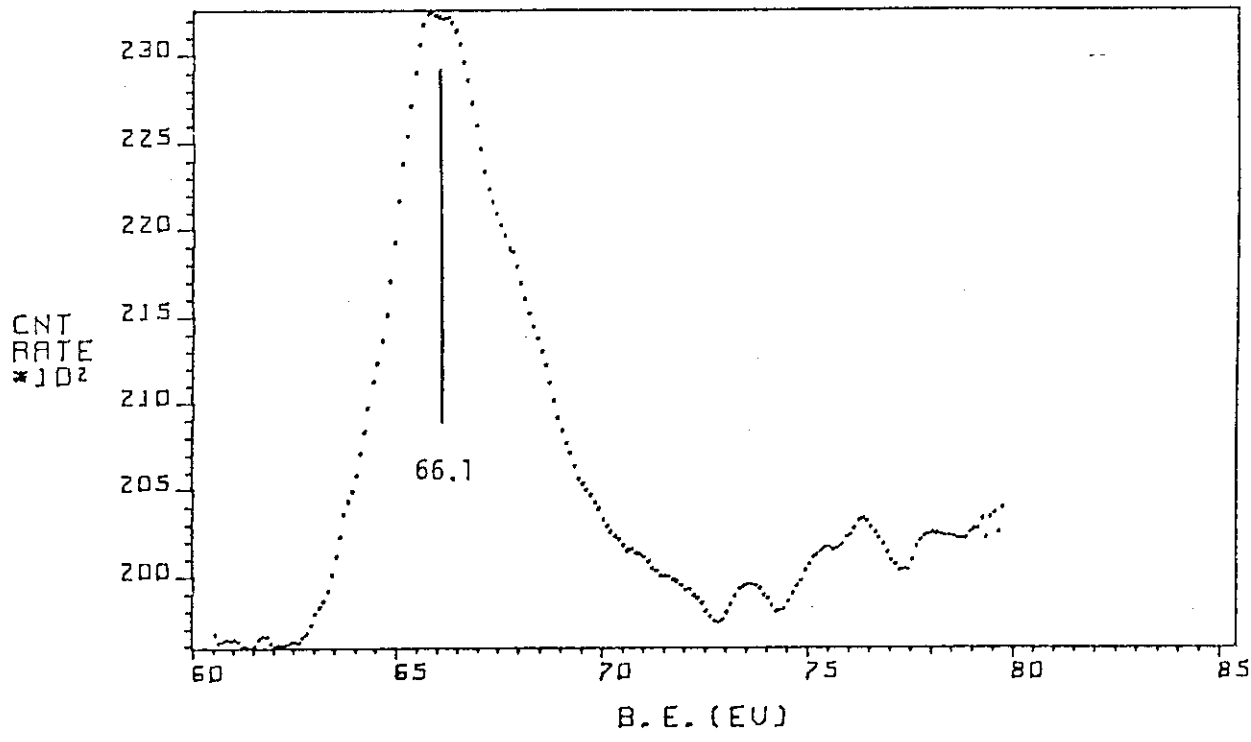

Fig. 35 V3s XPS spectrum of V_{fl}.

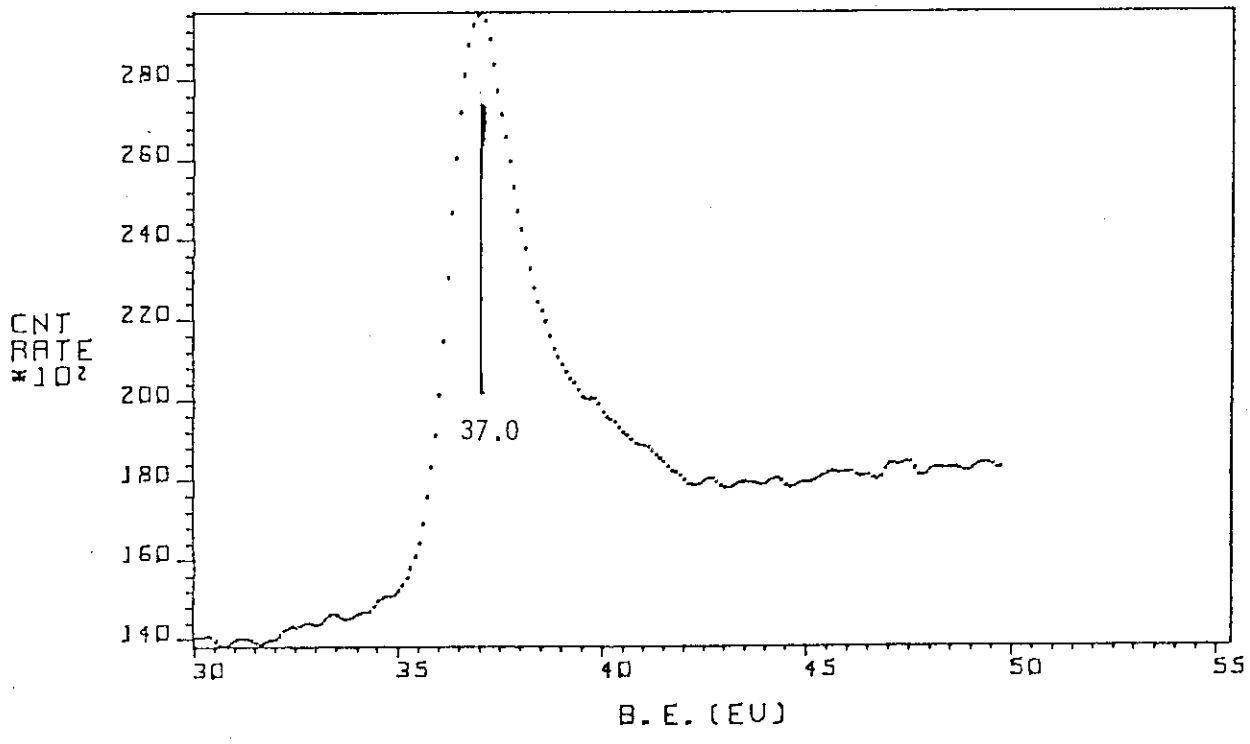

Fig. 36 V3p XPS spectrum of V_{fl}.

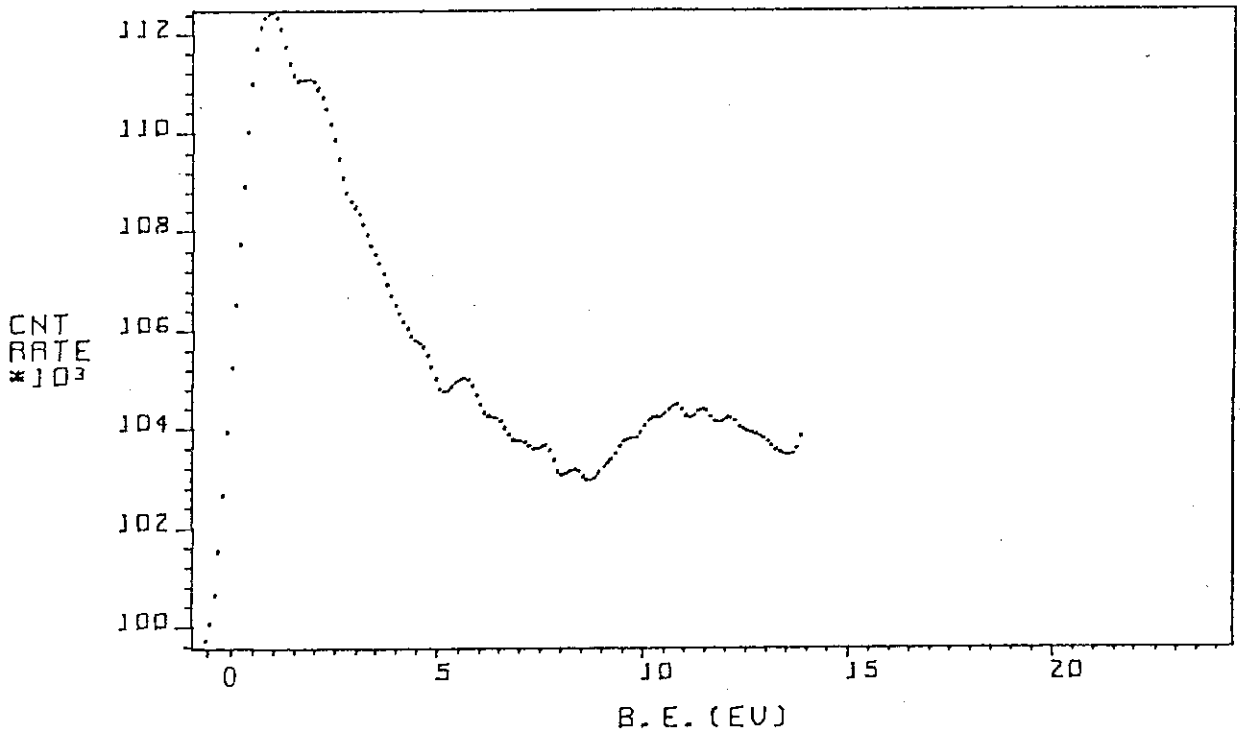

Fig. 37 Valence-band spectrum of V_{fl}.

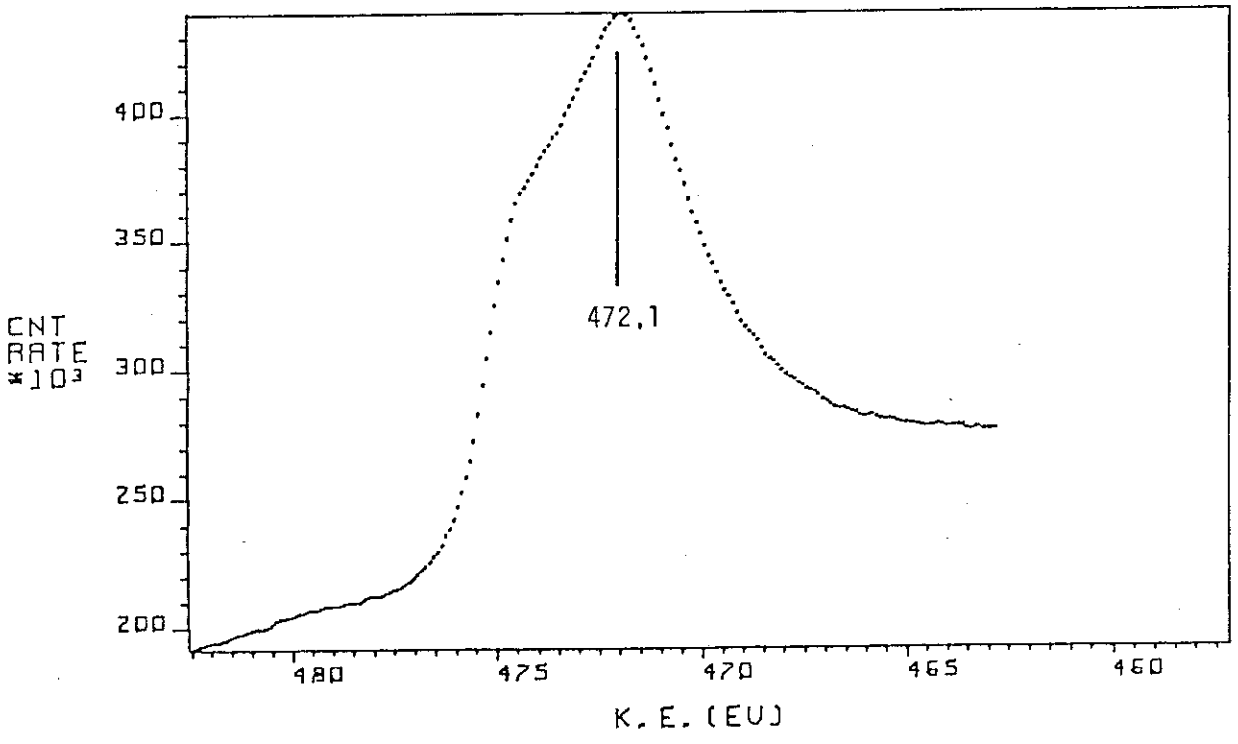

Fig. 38 $L_3M_{2,3}M_{2,3}$ XAES spectrum of V_{fl}.

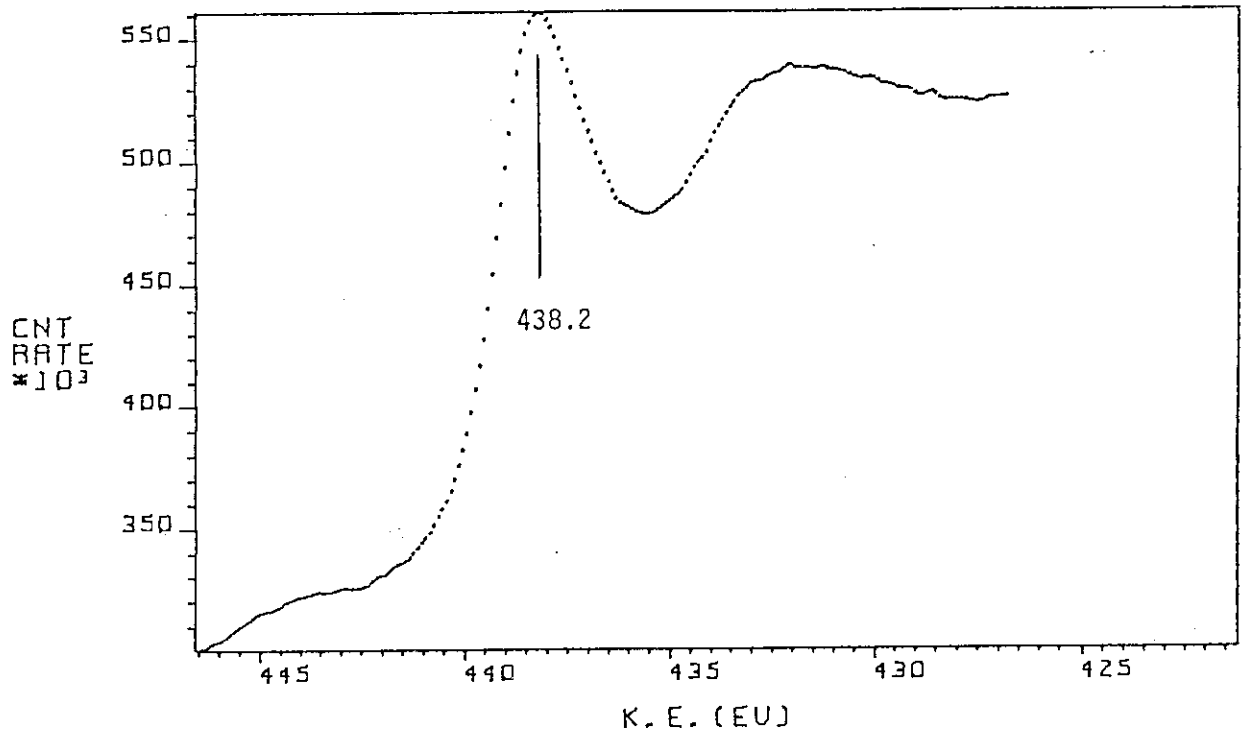

Fig. 39 $L_3M_{2,3}V$ XAES spectrum of V_{fl}.

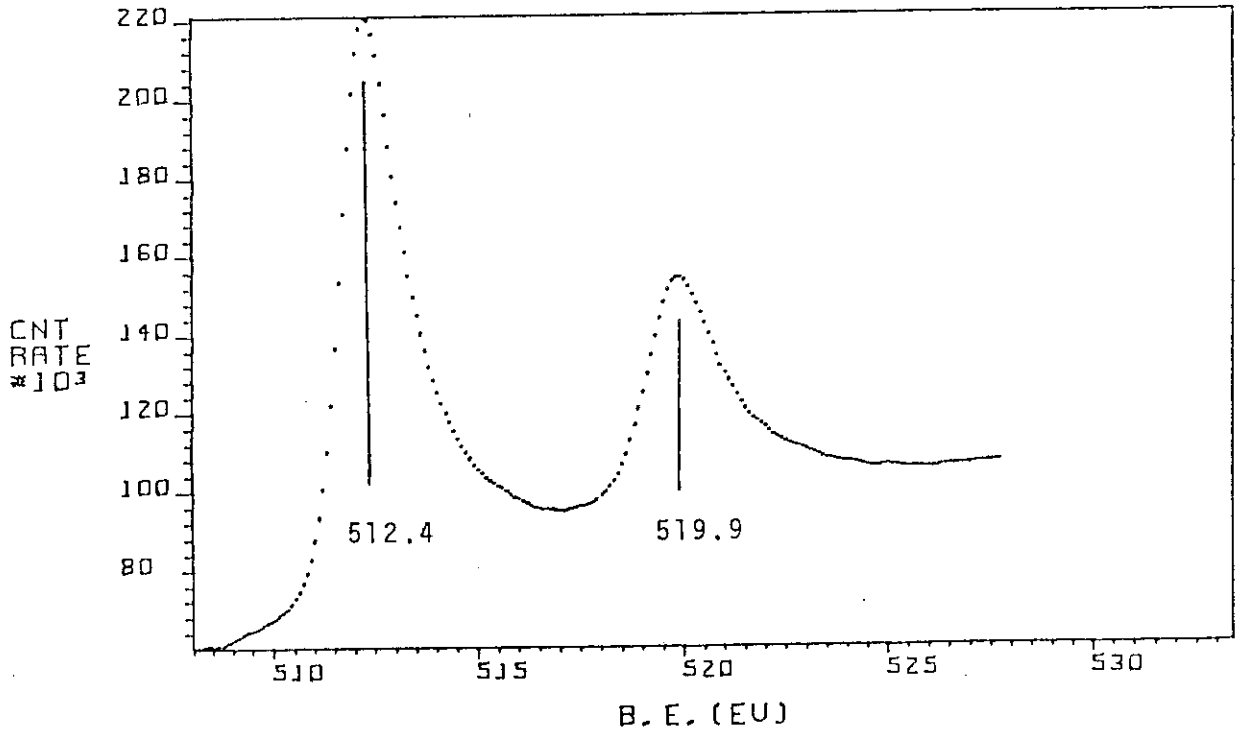

Fig. 40 V2p XPS spectrum of V_{et}.

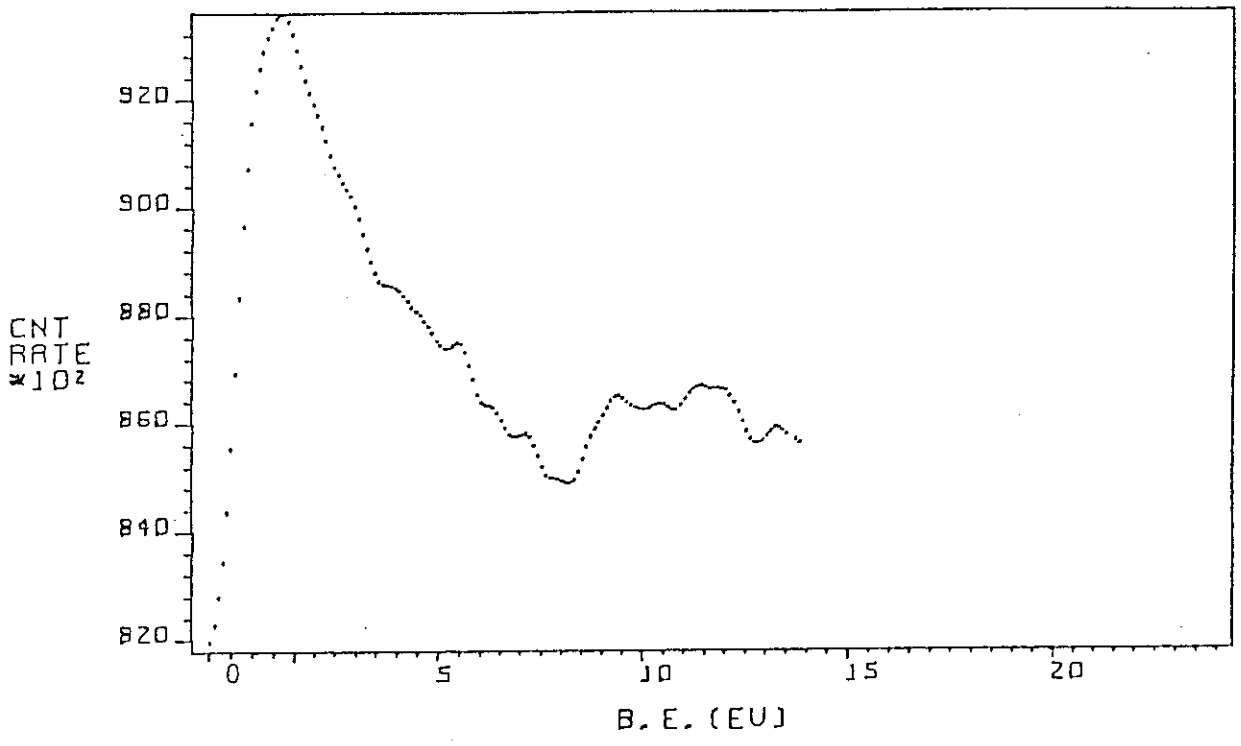

Fig. 41 Valence-band spectrum of V_{et}.

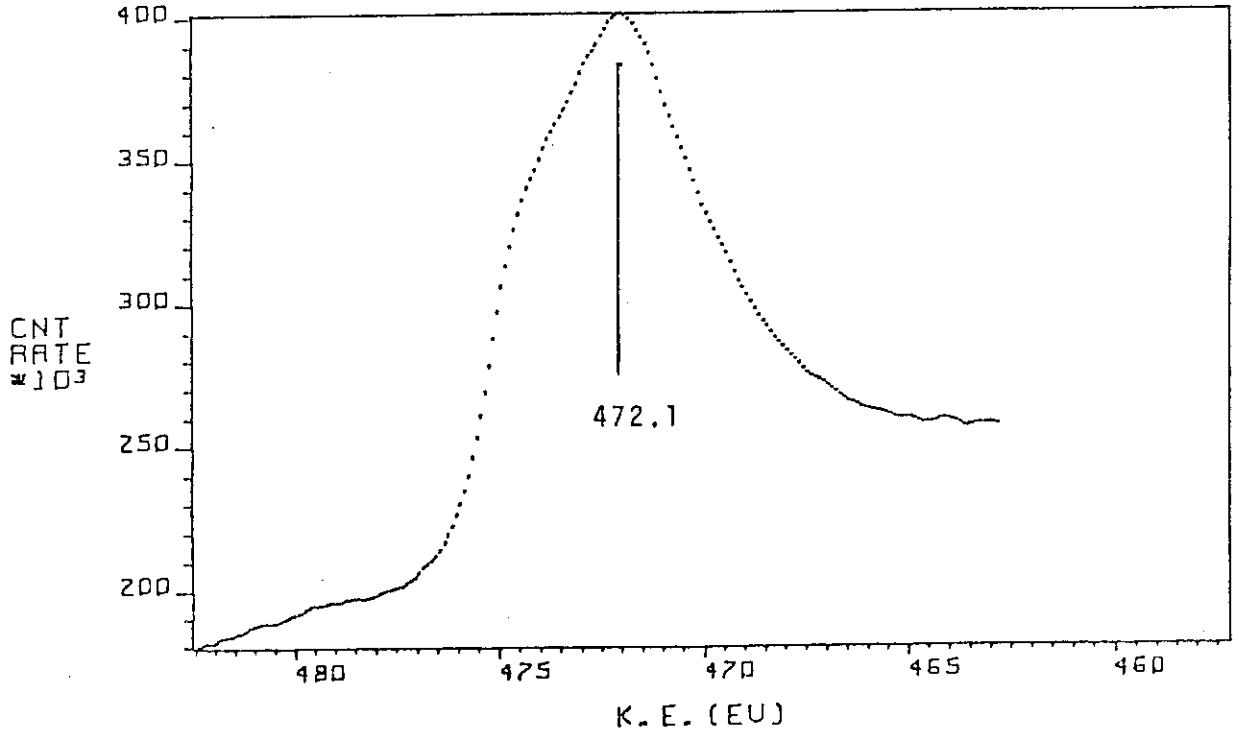

Fig. 42 $L_3M_{2,3}M_{2,3}$ XAES spectrum of V_{et}.

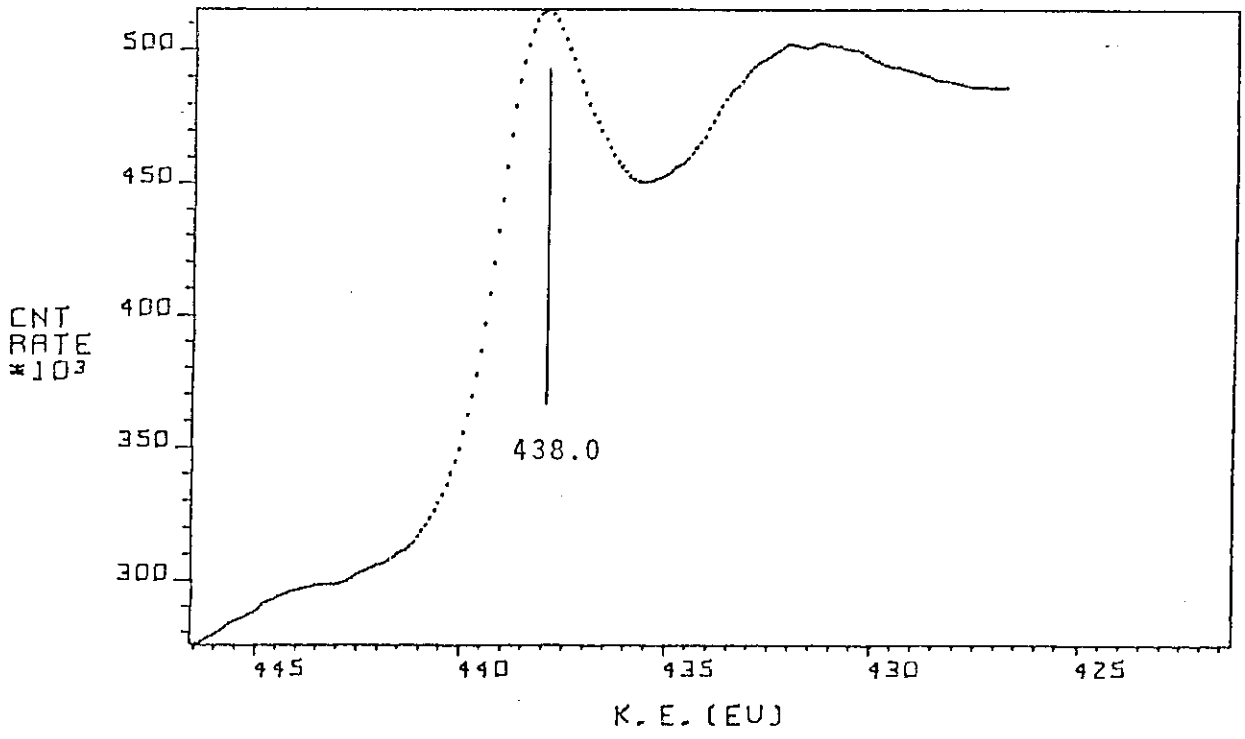

Fig. 43 $L_3M_{2,3}V$ XAES spectrum of V_{et}.

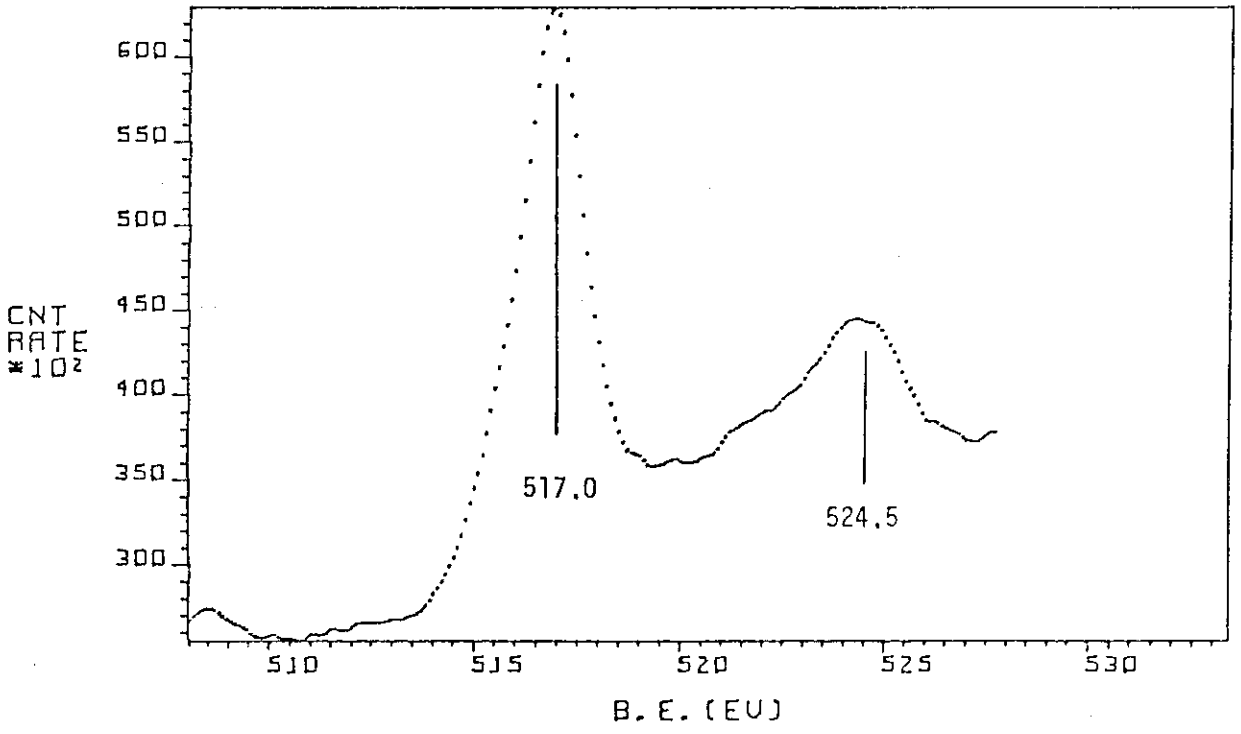

Fig. 44 V2p XPS spectrum of V_2O_5.

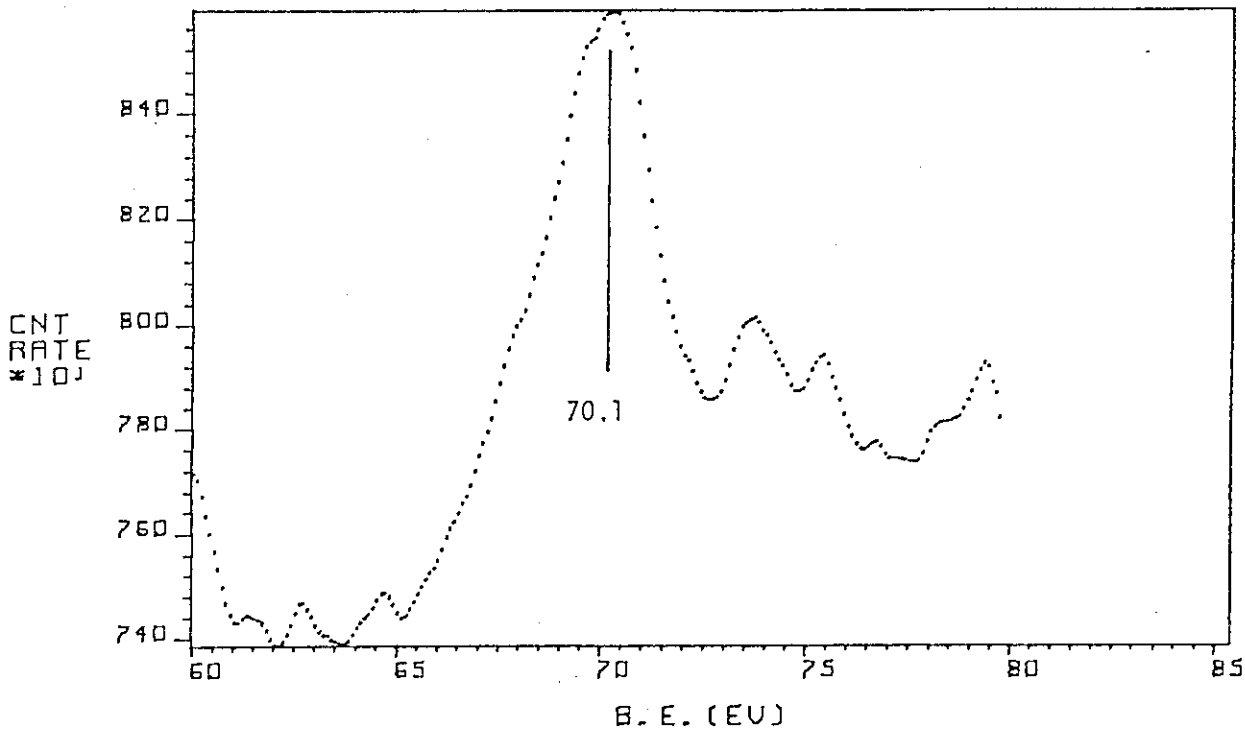

Fig. 45 V3s XPS spectrum of V_2O_5.

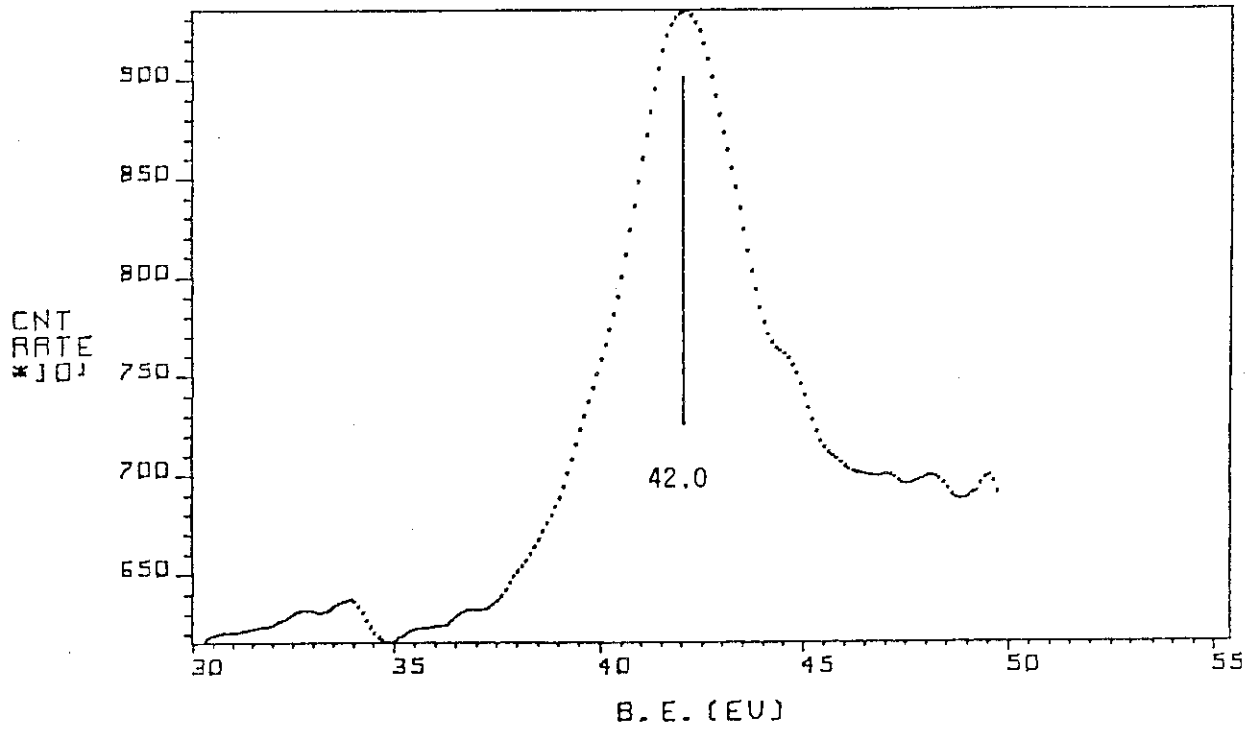

Fig. 46 V3p XPS spectrum of V_2O_5.

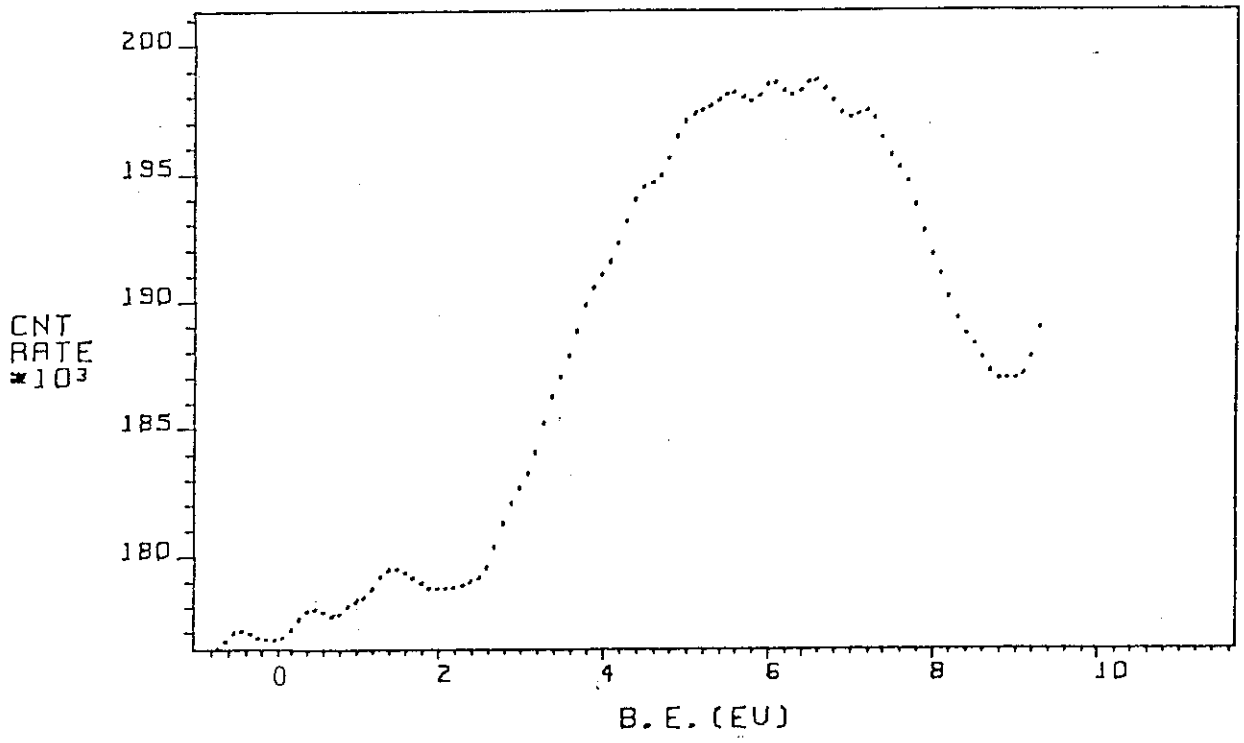

Fig. 47 Valence-band spectrum of V_2O_5.

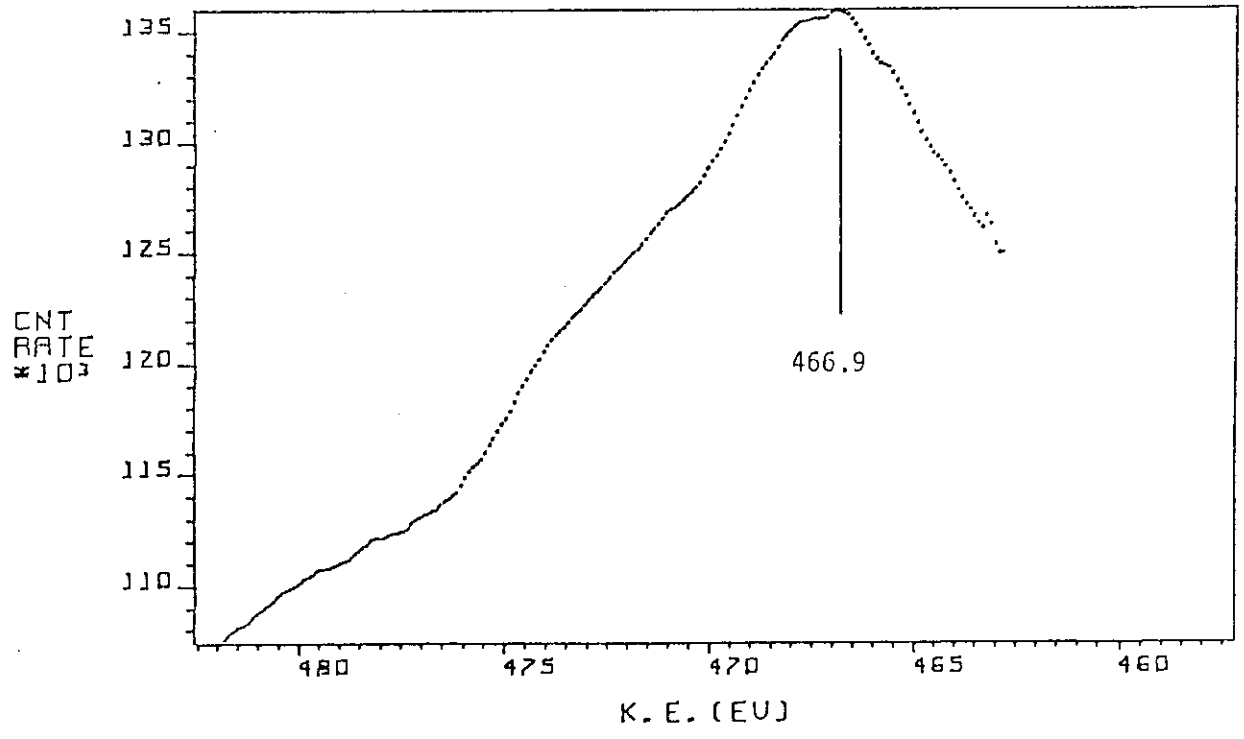

Fig. 48 $L_3M_{2,3}M_{2,3}$ XAES spectrum of V_2O_5.

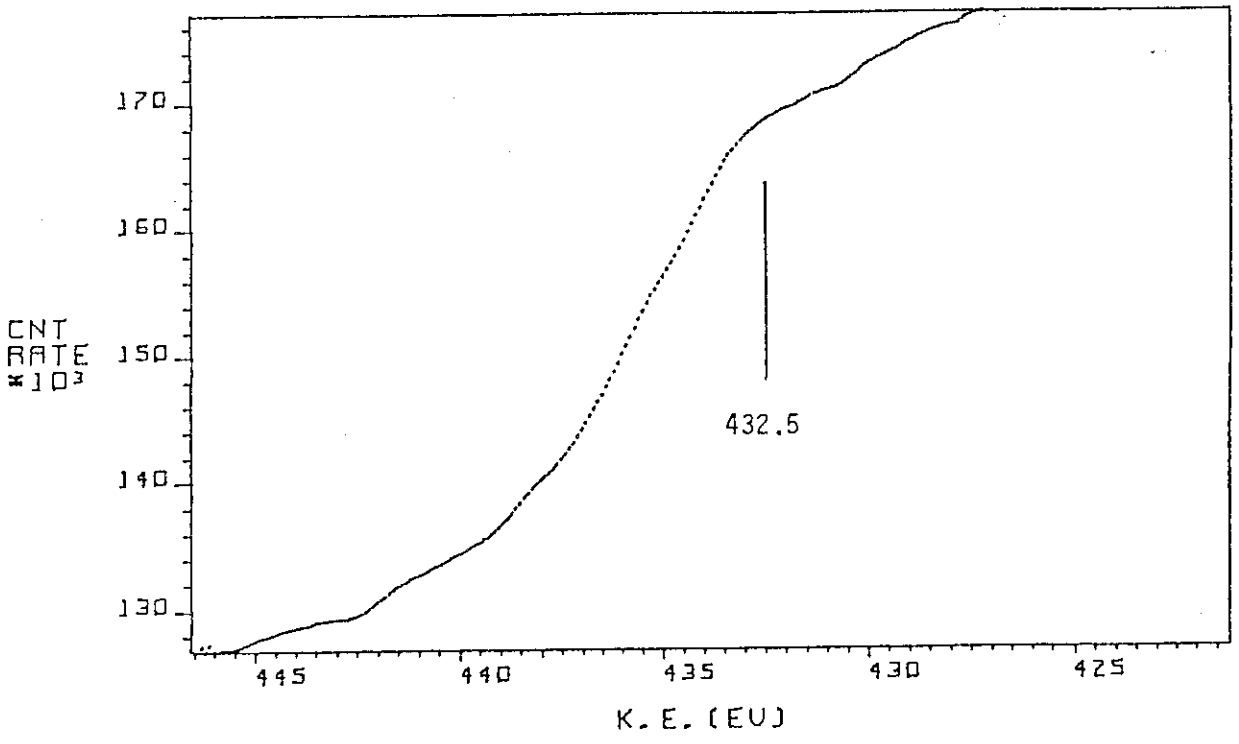

Fig. 49 $L_3M_{2,3}V$ XAES spectrum of V_2O_5.

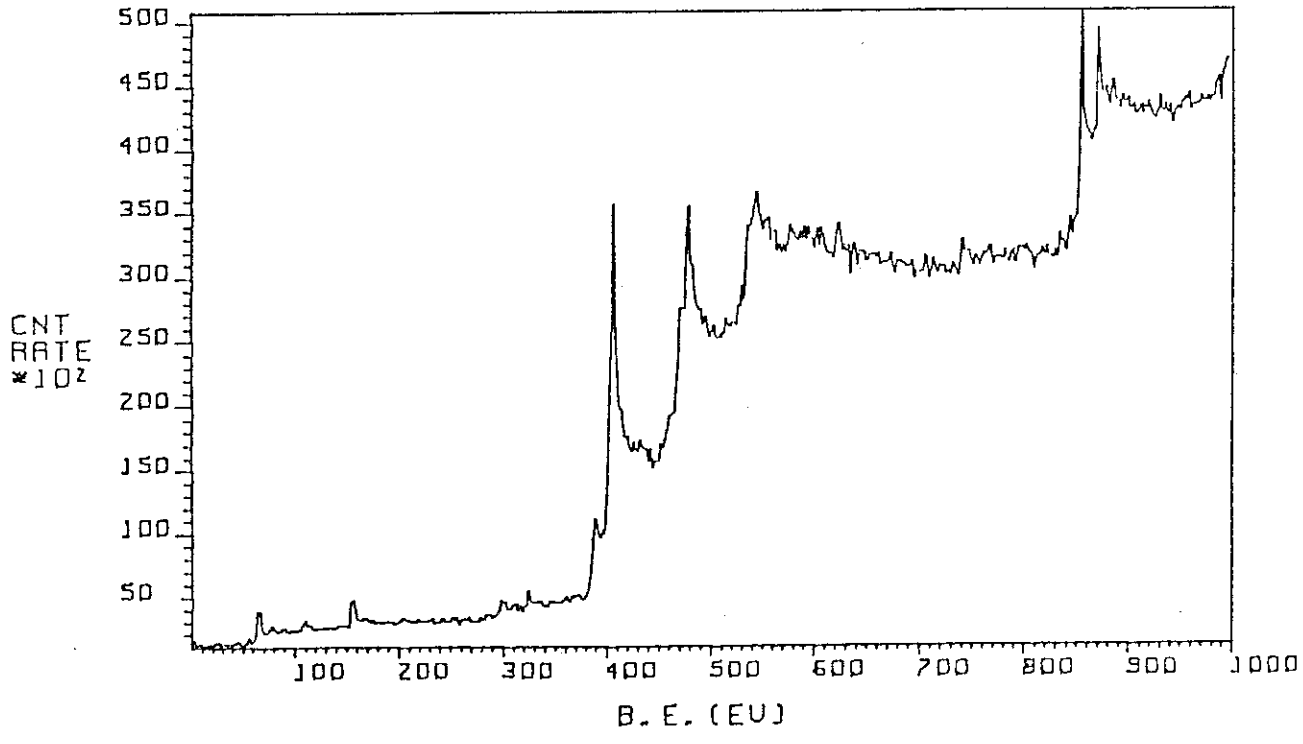

Fig. 50 XPS wide scan of Ni_{fl}.

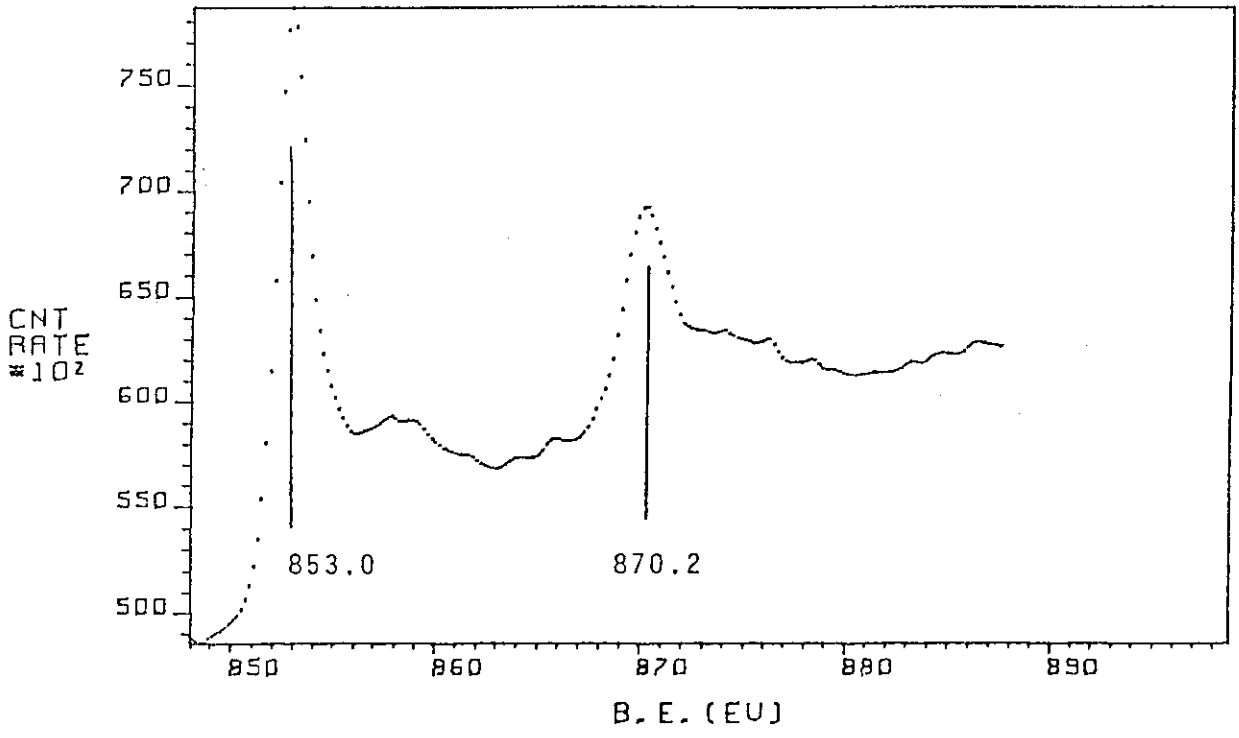

Fig. 51 Ni2p XPS spectrum of Ni_{fl}.

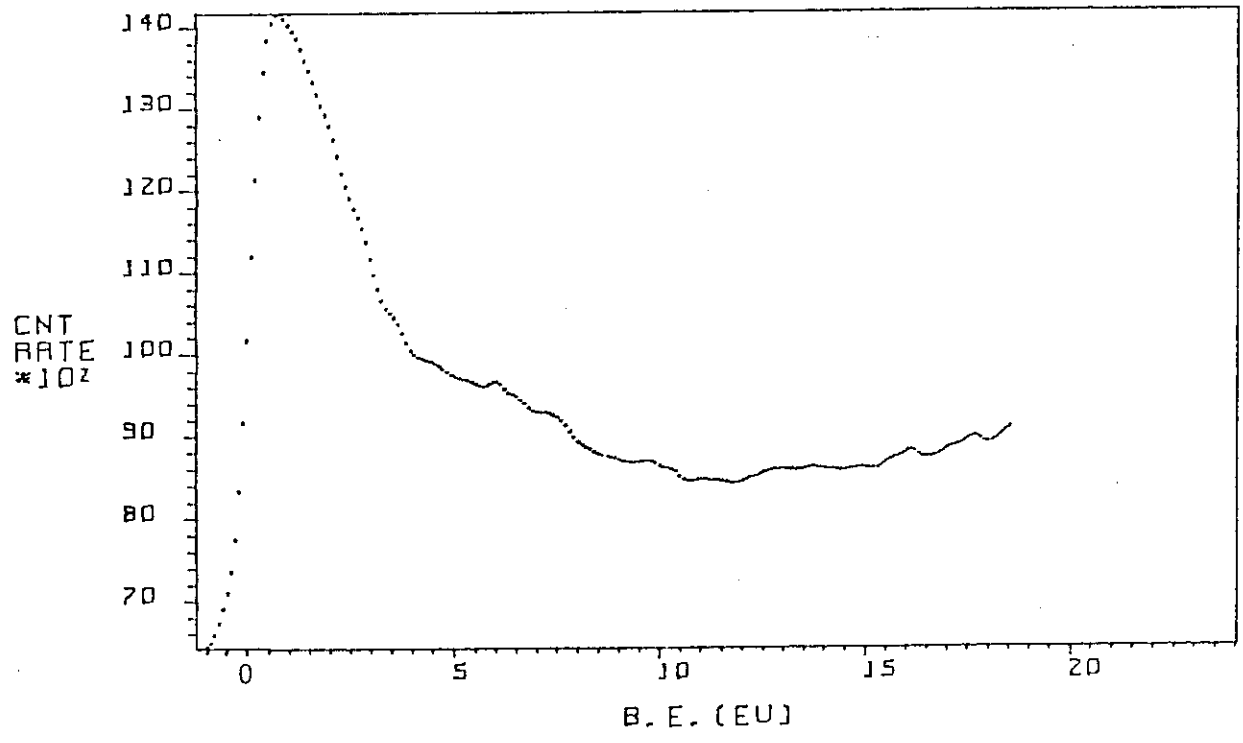

Fig. 52 Valence-band spectrum of Ni_{fl}.

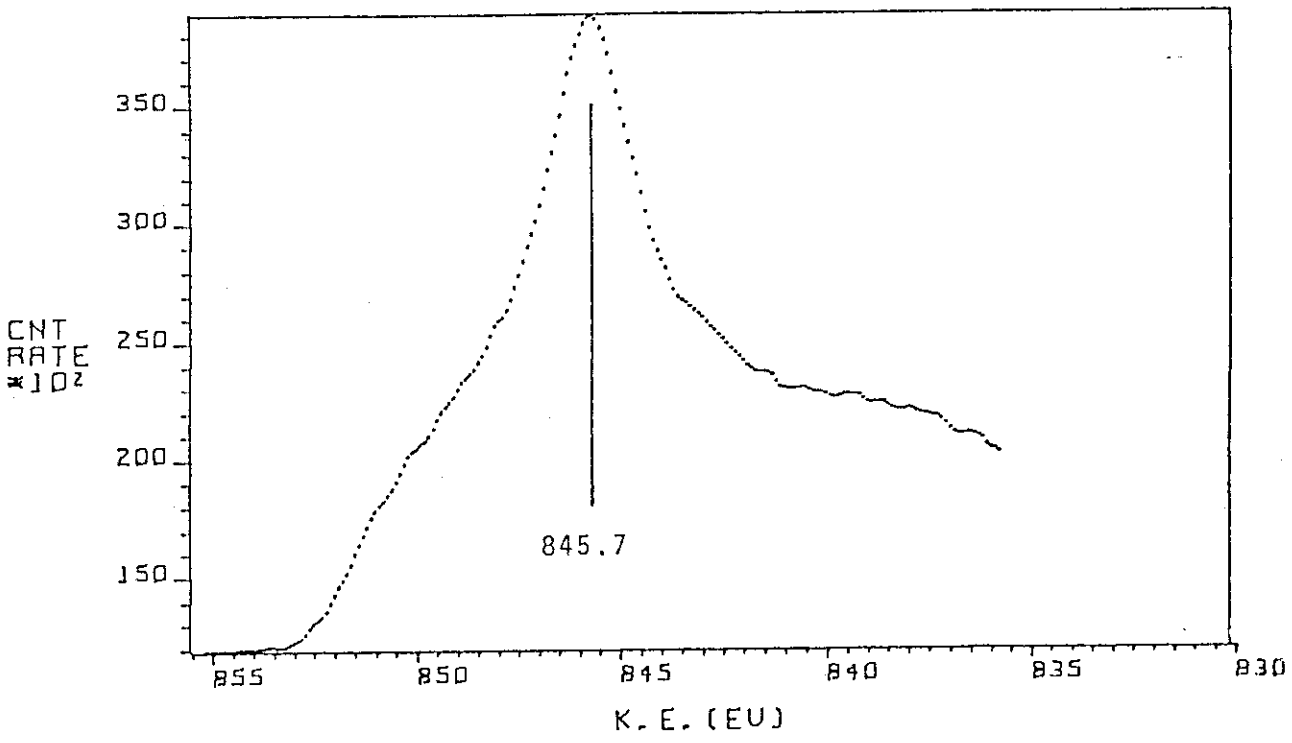

Fig. 53 $L_3M_{2,3}M_{2,3}$ XAES spectrum of Ni_{fl}.

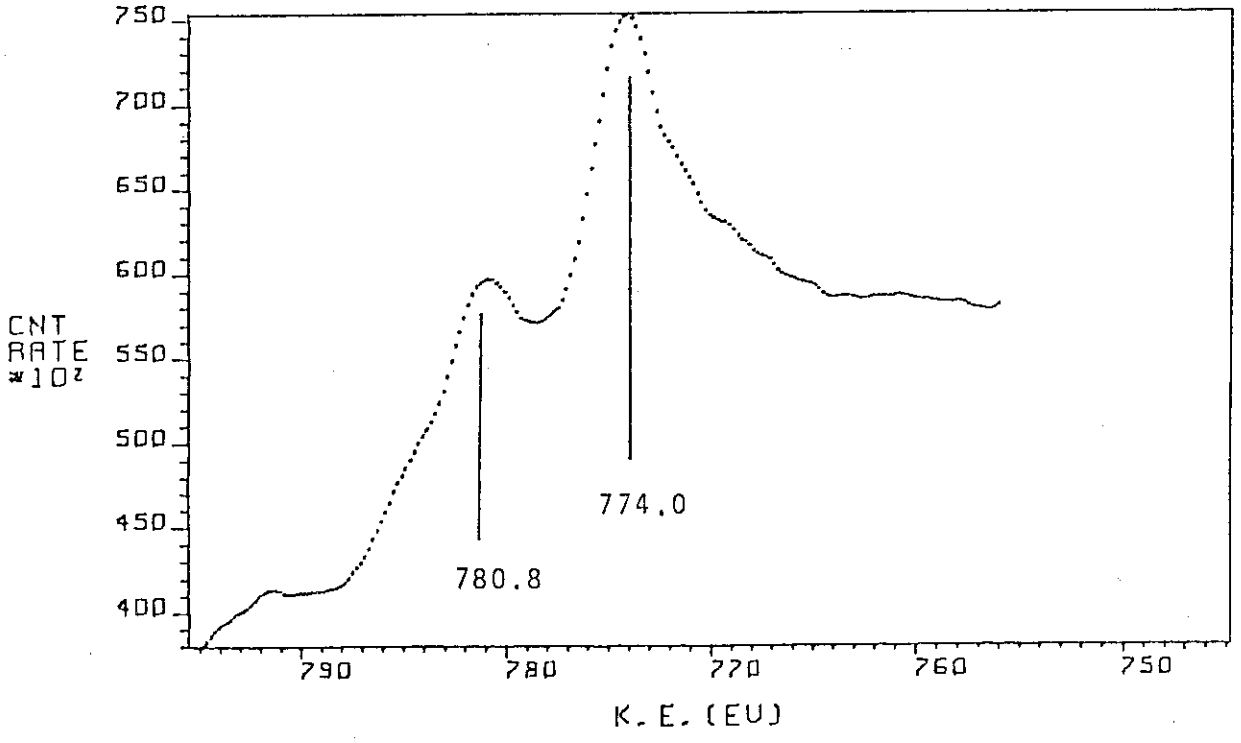

Fig. 54 $L_3M_{2,3}V$ XAES spectrum of Ni_{fl}.

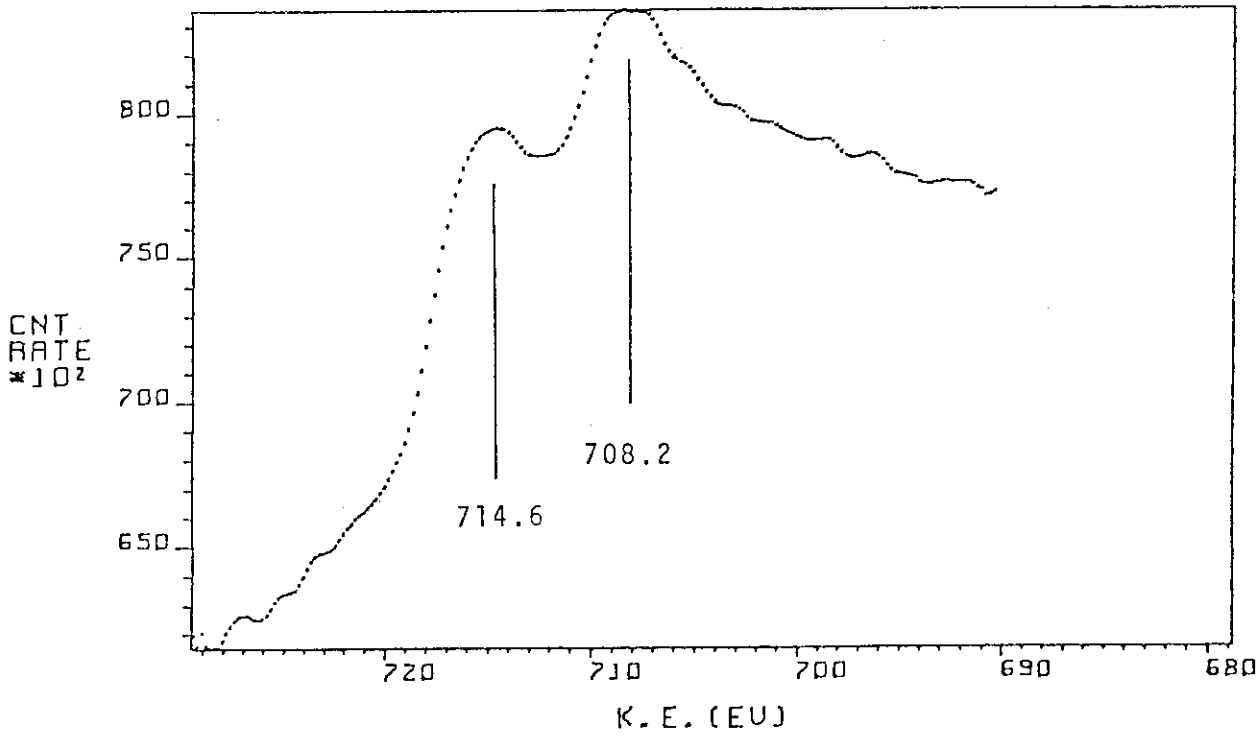

Fig. 55 L_3VV XAES spectrum of Ni_{fl}.

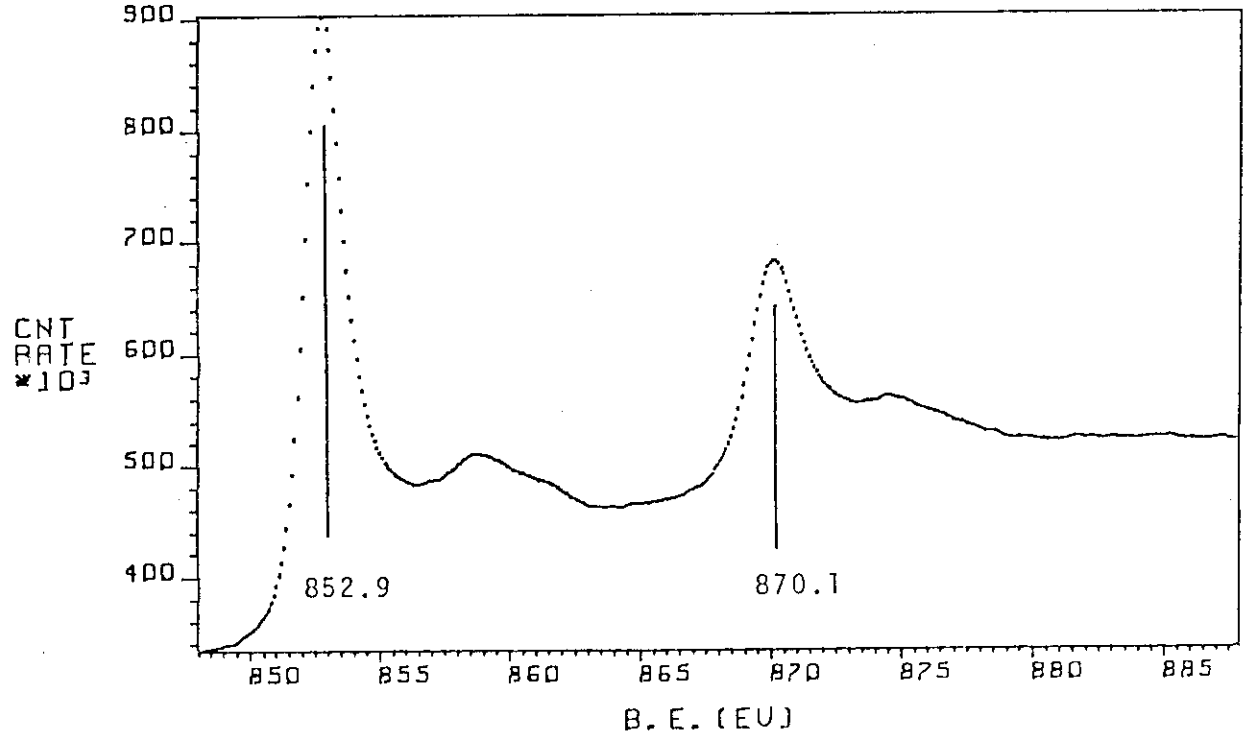

Fig. 56 Ni2p XPS spectrum of Ni_{et}.

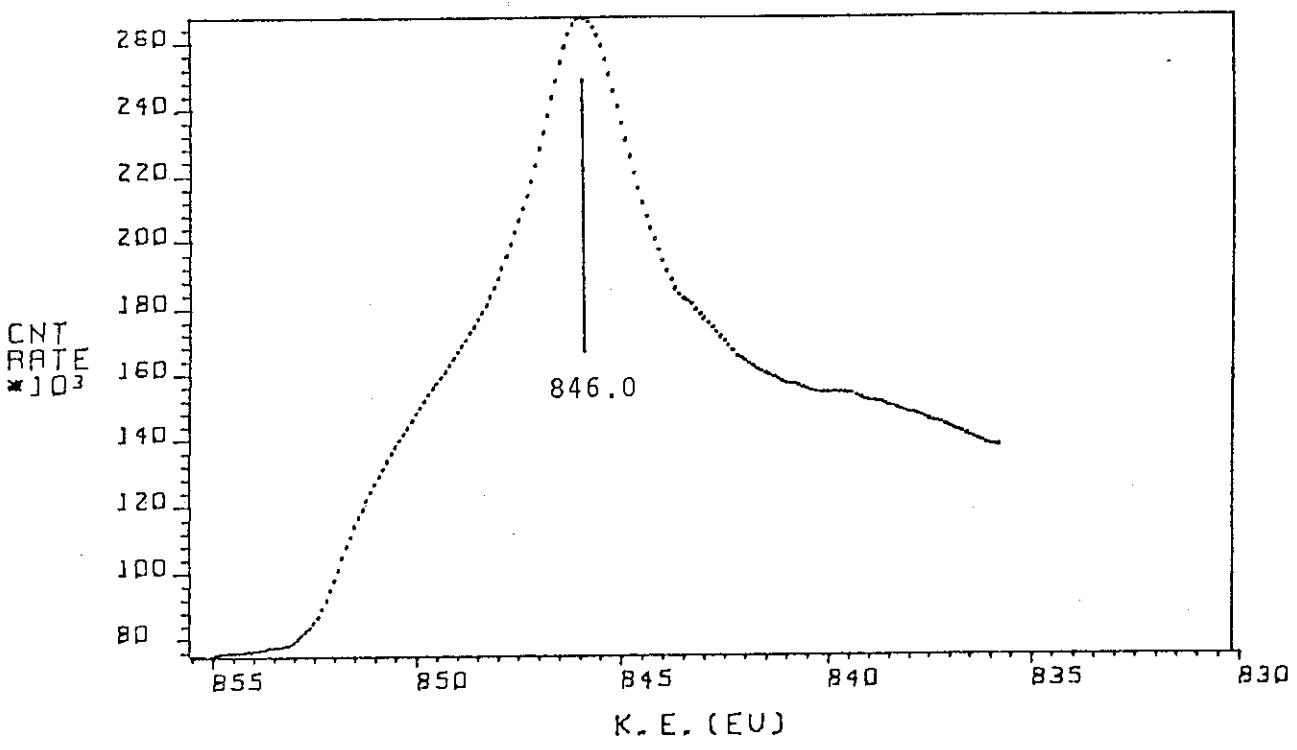

Fig. 57 L_3VV XAES spectrum of Ni_{et}.

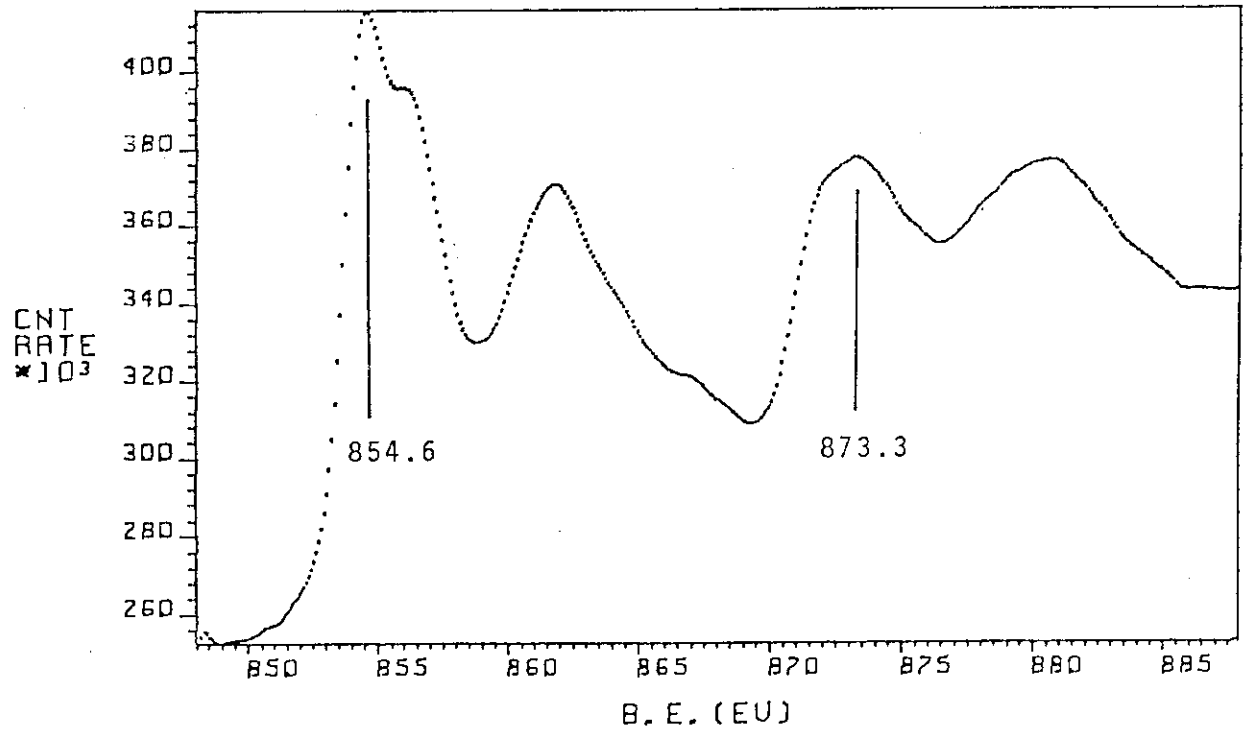

Fig. 58 Ni2p XPS spectrum of NiO.

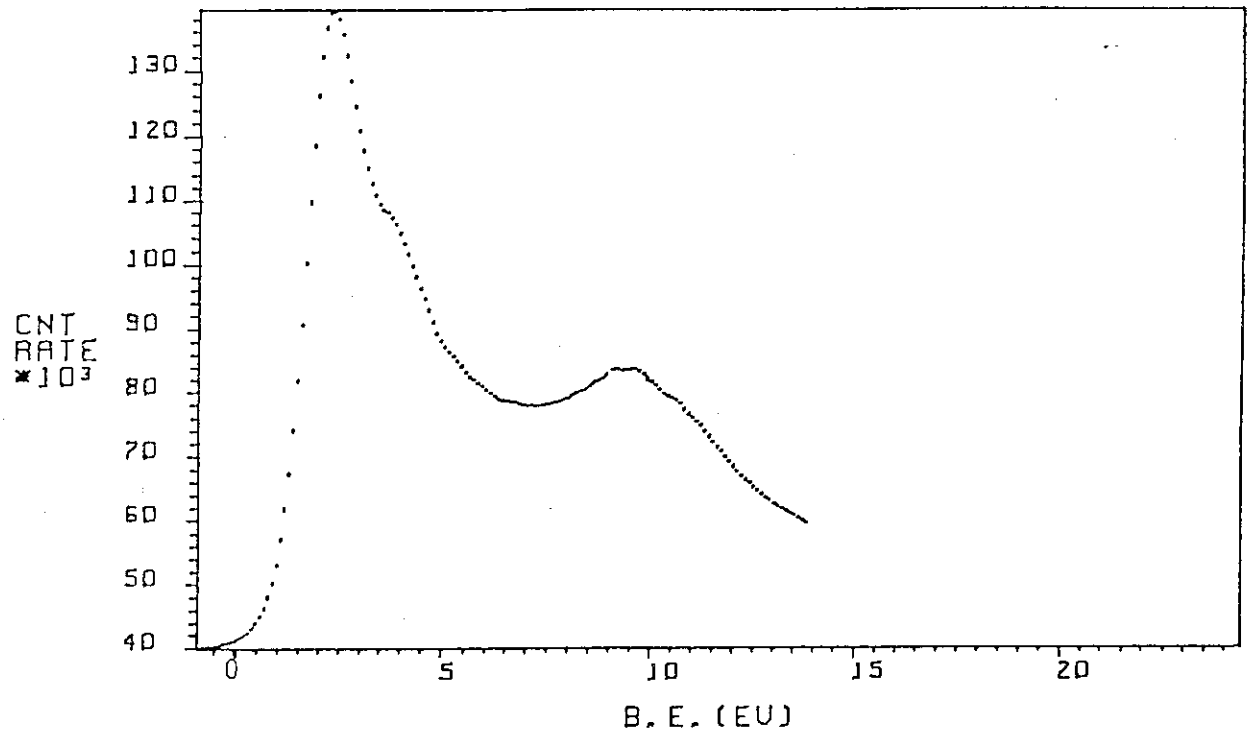

Fig. 59 Valence-band spectrum of NiO.

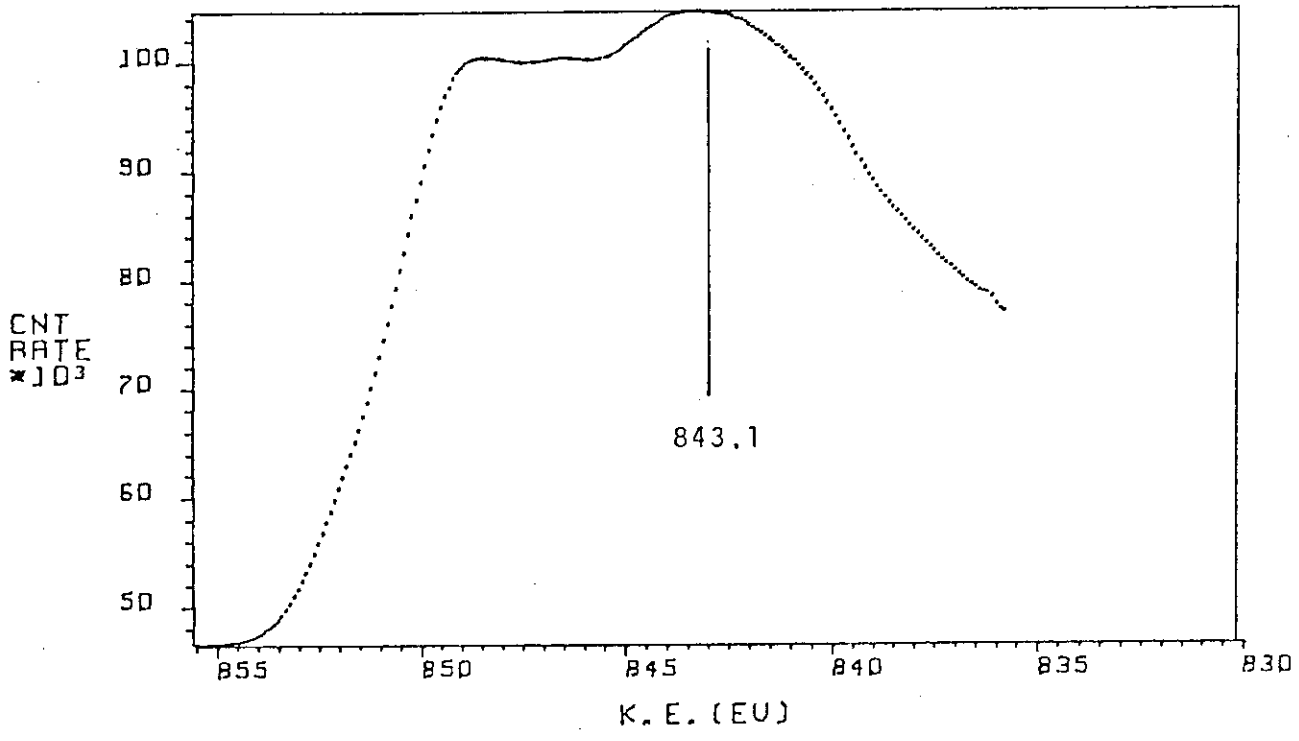

Fig. 60 L_3VV XAES spectrum of NiO.